Louisiana State University
LSU Digital Commons

LSU Master's Theses | Graduate School

2013

Aggregation of uncontrolled fluids during catastrophic system failures in offshore environments

James Thomas Stiernberg
Louisiana State University and Agricultural and Mechanical College, j.stiernberg@gmail.com

Follow this and additional works at: https://digitalcommons.lsu.edu/gradschool_theses

 Part of the Petroleum Engineering Commons

Recommended Citation
Stiernberg, James Thomas, "Aggregation of uncontrolled fluids during catastrophic system failures in offshore environments" (2013). *LSU Master's Theses*. 2178.
https://digitalcommons.lsu.edu/gradschool_theses/2178

This Thesis is brought to you for free and open access by the Graduate School at LSU Digital Commons. It has been accepted for inclusion in LSU Master's Theses by an authorized graduate school editor of LSU Digital Commons. For more information, please contact gradetd@lsu.edu.

AGGREGATION OF UNCONTROLLED FLUIDS DURING CATASTROPHIC SYSTEM FAILURES IN OFFSHORE ENVIRONMENTS

A Thesis

Submitted to the Graduate Faculty of the
Louisiana State University and
Agricultural and Mechanical College
in partial fulfillment of the
requirements for the degree of

Master of Science in Petroleum Engineering

in

The Craft and Hawkins Department of Petroleum Engineering

by
James Stiernberg
B.S., The University of Texas at Austin, 2009
August 2013

Acknowledgements

I would like to thank my parents for supporting me through my undergraduate studies and always backing me up in the decisions I made. Lina Bernaola has also made a significant impact on my life and I owe her a great deal for helping me see the completion of this work. I am grateful to the Louisiana State University and the faculty in the Craft and Hawkins Department of Petroleum Engineering in particular for giving me the opportunity to pick up my academic career again after working in the field. Regarding my admission, I am indebted to those who put their reputation on the line by vouching for me during the application process; namely, Dr. Russell Johns, Dr. Neil Deeds, and Dr. Bayani Cardenas. I have learned a great deal from all three and I cannot underline their contribution to my success enough.

Dr. Richard Hughes and Dr. Mayank Tyagi are inspiring instructors and dedicated advisors both and, without their help, this work would not have been possible. I would like to extend my gratitude towards Dr. Julius Langlinais and also Shell for financial support in this research and my academic endeavors here at LSU. Dewayne Anderson at SPTgroup has been invaluable with understanding OLGA® and troubleshooting simulation errors that came up. Venu Nagineni has been my friend and is now also my connection over at Calsep; I'm grateful for all the help he offered me concerning PVTsim®. Finally, I'd like to thank Muhammad Zulqarnain for some guidance during my studies as well as providing excellent pictures of real oilfield equipment.

Table of Contents

Acknowledgements ii

List of Tables v

List of Figures vi

Nomenclature viii

Abstract x

Chapter 1: Introduction 1
1.1 Motivation for Research 1
1.2 Thesis Outline 1

Chapter 2: Considerations and Problem Setup 3
2.1 Conceptualizing the Scenario 3
2.2 Reservoirs and Fluids 3
2.2.1 Influence of Formation Parameters 4
2.2.2 Fluid Properties and Flow Performance 7
2.3 Impact of Production Tubing 9
2.3.1 Installed Components 10
2.3.2 Geometry of Tubulars 12
2.4 Preliminary Conclusions from Performance Relationships 12

Chapter 3: Theory of Implemented Tools 15
3.1 Nodal Analysis 15
3.2 Simulation Software Packages OLGA® and PVTsim® 15
3.2.1 The Flow Assurance Software OLGA® 17
3.2.2 Phase Behavior and PVTsim® 19

Chapter 4: Leak Geometry and Discharge Coefficient 23
4.1 Sheared or Parted Pipe 24
4.1.1 Gilbert Discharge Equation 24
4.1.2 Validity of the Gilbert Equation and Other Methods for Seafloor Leaks 25
4.2 Leaking from a Failed Flange Connection 29
4.3 Arbitrary Hole Shape and Modifications to the Flow Equation 31

Chapter 5: Method and Procedure 34
5.1 OLGA® Flow Model 34
5.2 Phase Behavior Studies 37

Chapter 6: Discussion and Results 39
6.1 Commingling Fluids with Various Pressures 39
6.2 Influence of Mixture Ratio on Fluid Properties 40
6.3 Compositional Effects in Simulation 43

6.3.1 Effect of Undersaturated Oil Coming in Contact with Condensate Gas 43
6.3.2 Estimating GOR with Heptanes Plus Fraction 46

Chapter 7: Conclusions 54
7.1 Performance Relationships Dependencies 54
7.2 Position and Shape of Leak 54
7.3 A New Correlation When Information is Scarce 55
7.4 Suggestions on Future Work 55

Bibliography 58

Appendix 63
A. Fluid Bank 63
B. Heat-Transfer Coefficient Calculations 65

Vita 69

List of Tables

1 Original Reservoir Properties Used in Sensitivity Study 6

2 Results of TPR Sensitivity Study 12

3 Coefficients Proposed for the Gilbert Flow Equation 24

4 Relative Differences of Various Discharge Estimation Methods..... 26

5 Liquid Rates Resulting from Different Pressures and Gas-Liquid Ratios 31

6 Ratios used in Condensate-Oil Mixtures..... 37

7 Justification of Mixture Ratios Used in the PVT Study..... 38

8 Liquid Leak Rates (BOPD) of Condensate-Black Oil Mixtures..... 43

9 Gas Leak Rates (Mcf/D) of Condensate-Black Oil Mixtures 44

10 Gas-Liquid Ratios (ft^3/bbl) from the Gas Tieback Only..... 45

11 Percent Change in Gas-Liquid Ratios from Wellheads to Leak Point..... 46

12 Condensate Fluids Used in Studies and Some of Their Properties..... 63

13 Black Oils Used in Studies and Some of Their Properties 64

14 Well Profile and Material Properties Used in Thermal Calculations 66

List of Figures

1 Schematic of Simplified Confluence and Leak Section 4

2 Parametric Study of Reservoir Properties. 7

3 Parametric Study of Formation Fluid 8

4 Block Diagram of Iterative Solution 10

5 Parametric Study of Tubing Performance Relationship 11

6 Overview of Important Variables in Hydrocarbon Production 13

7 Duns and Ros Flow Pattern Map 16

8 Examples of Sufficient and Invalid Discretizations 18

9 Failure Mode Tree for Deep Water Wells 23

10 Discharge Model Comparisons 26

11 Choke Model as Used in OLGA® 28

12 Wellhead Flange Diagram 30

13 Examples of Flange Varieties and Connections for Subsea Applications 30

14 Arbitrary Hole Geometry in Ruptured Pipe 33

15 Diagram of Gathering System as Modeled in OLGA® Simulation 35

16 Well Cross-Section Showing Dimensions of Tubulars and Cement 36

17 Gas-Liquid and Formation Volume Factor vs. Liquid Flow Rate 40

18 Phase Diagrams for Molar Mixtures of Condensate and Black Oil 41

19 90% Quality Lines for a Condensate-Black Oil Mixture 42

20 Gas-Liquid Ratio Sampling Points within the OLGA® Model 45

21 Initial GOR Veresus Heavy Components Fraction 47

22 Fitting Simulation Data to the Overall Fluid Trend 48
23 Comparing Various Methods for Predicting GOR 49
24 Drift in Heptanes-Plus Prediction While Developing Correlation 51
25 Correlation Procedure Diagram 52
26 Hierarchical Mixing 53
27 CFD Model of Well Flange Leak Point 56

Nomenclature

Symbols	Description	SI Units	Field Units
γ	Euler constant = 0.5772	-	-
Δ	Change in some variable	-	-
ε	Coefficient of emissivity	-	-
κ	Specific Heat Ratio	-	-
μ	Viscosity	P or Pa·s	$lb_m/ft \cdot s$
ρ	Density	kg/m^3	lb_m/ft^3
φ	Fugacity coefficient	Pa	psi
C	Courant (CFL) number	-	-
C_D	Discharge coefficient	-	-
c_t	Total isothermal compressibility	Pa^{-1}	psi^{-1}
g	Gravitational acceleration	m/s^2	ft/s^2
GOR/GLR	Gas-oil/gas-liquid ratio	m^3/m^3	cf/bbl
h_c	Convective heat-transfer coefficient	W/m^2-°C	Btu/ft^2-hr-°F
h_r	Radiative heat-transfer coefficient	W/m^2-°C	Btu/ft^2-hr-°F
h_{res}	Reservoir thickness	m	ft
h_{ti}	Conductive heat-transfer coefficient	W/m^2-°C	Btu/ft^2-hr-°F
H_L	Liquid holdup	-	-
k	Thermal conductivity	W/m-°C	Btu/ft-hr-°F
K	Permeability	m^2	mD
N	Liquid velocity number	-	-
N_d	Diameter number	-	-
N_l	Liquid viscosity number	-	-
n_i	Moles of species *i*	-	-
P or p	Pressure	N/m^2	lb_f/ft^2
Pr	Prandtl number	-	-
Q	Volumetric Flow Rate	m^3/s	ft^3/s
r	Radius	m, cm	ft, inches
RN	Gas velocity number	-	-
Re	Reynolds number	-	-
SG	Specific Gravity	-	-
T	Time	days	days
u	Velocity	m/s	ft/s
V	Volume	m^3	ft^3
x	Spatial discretization length	m	ft
Z	Compressibility factor	-	-

Subscripts	Description
ann	Annulus
cem	Cement
ci, co	Inner and outer casing surface
p	Phase
res	Reservoir conditions
s	Source
sep	Separator conditions
sg	Superficial gas [velocity]
sl	Superficial liquid [velocity]
ti, to	Inner and outer tubing surface
wf	Flowing well
wh	Wellhead

Abstract

Safety culture relating to offshore operations has shifted since the Deepwater Horizon blowout and resulting oil spill. This incident has prompted the research of high volume spills during all stages of hydrocarbon exploration and production. This study particularly covers the interactions of wells and offshore networks as they pertain to situations where a release of reservoir fluids to the environment is occurring. Primary concerns of this investigation are stream confluences, leak modeling, and fluid behavior; the first two will be handled with various numerical software packages (OLGA®, CFD, and nodal analyses) while the later will require more rigorous treatment and a combination of these tools with dedicated phase behavior software (such as PVTsim®). This research will combine with risk analysis work being done by others to identify high-priority system failure scenarios.

The focus in modeling high-volume leaks thus far has been placed upon reservoir properties, geology and modeling the most uncertain things when this research shows that the most influential variables for particular reservoirs lie within the flow path. When operating offshore, wells connect to subsea manifolds or other junctions to form unforeseen mixtures of crude oils; these combined fluids dictate the outcome of potentially devastating releases offshore.

Flow rates through chokes have been modeled using only a few parameters, namely the pressure, choke size and the gas-liquid ratio (GLR). The leak considered herein will choke flow and create a back pressure, which will control how fluids move from the reservoir to wellhead. A properly tuned equation of state can predict the GLR fairly well, but falls short when attempting to combine the GLR of two or more fluids. A correlation is proposed to allow for more accurate leak models when only simple fluid properties are known, such as the heptanes-plus fraction.

Chapter 1
Introduction

1.1 Motivation for Research

Drilling frontiers have continuously expanded due to the demand for oil. Over 44,000 wells have been drilled in the Gulf of Mexico since 1947 (Forrest et al., 2005) and it is in the deepest of these wells that higher pressure and higher temperature reservoirs are typically located. Large reservoirs can be found at such extremes, but the capital investment to discover and develop these reservoirs is enormous and increasing. It is also costly to maintain and operate the platforms that produce the hydrocarbons to surface. Limited slots for wells on a platform provide an impetus to develop satellite fields, which aggregate produced fluids before allowing them to flow to facilities at the surface. However, extending the working life of a platform in this manner may carry unintended consequences and risks. Each node or junction in the network of flow lines from the infrastructure beginning at the seafloor and continuing up to the platform is a possible leak point. Knowing the rate of each fluid phase at these junctions and the duration of any leak is essential to calculating the magnitude of the accident and predicting the environmental impact.

1.2 Thesis Outline

Presented herein are the results of simulations describing the aggregation of a number of reservoir fluids, with varying physical and chemical properties, in a subsea development. The goal is to model higher profile reservoirs, which would potentially be the most damaging upon unfettered release of their energy. Of particular interest is how these reservoirs would combine at confluences in different parts of the surface network. For instance, what happens when subsea safety valves fail below a single template and allow low and high gravity crudes to mix? Chapter

two begins by setting up such a generic scenario, discussing the types of reservoirs involved and the most important parameters responsible for pressure losses. Chapter three follows with more in-depth theory related to the methods and tools used in the present research. Parameters factoring into flow through a leak are discussed in chapter four. The choices of which correlation or physical model to use is described in chapter five on the procedures carried out in this study; the benefits and pitfalls of each item are exposed. A final discussion of the results concludes the work and offers suggestions on how future engineering designs can benefit.

Chapter 2
Considerations and Problem Setup

2.1 Conceptualizing the Scenario

The primary objective of the study is to understand how multiple sources of fluid can combine when fluid properties and flow path configurations are known. The leak, of unknown geometry and size, constrains effluent flow at a relatively low, hydrostatic pressure; there is a difference to consider between produced hydrocarbon and water within a pipeline versus said fluids escaping directly to the seafloor at hydrostatic conditions. A basic scenario will be used first to investigate the sensitivities of various parameters within the system and then an effort will be made to adjust this to more realistic setups.

2.2 Reservoirs and Fluids

Modeling two different reservoirs, containing disparate fluids, will be sufficient for the initial model and will provide some insight on how flow rates and void fractions are affected when these two entities are joined. To link them, two vertical, straight-hole wells are combined whereby their production paths are connected with a simple T-joint. A schematic of the system with variables of particular interest is presented in Figure 1 for clarification. Specific parameters of each reservoir will not, as it turns out, create the largest impact upon the flow rates of interest if the only types of reservoirs considered are those that are economically producible in deepwater fields. Relative flow rates, however, will primarily be determined by fluid properties. Well parameters, such as tubing diameter, will remain constant during this exercise; the sensitivity owing to the system's plumbing will be seen thereafter.

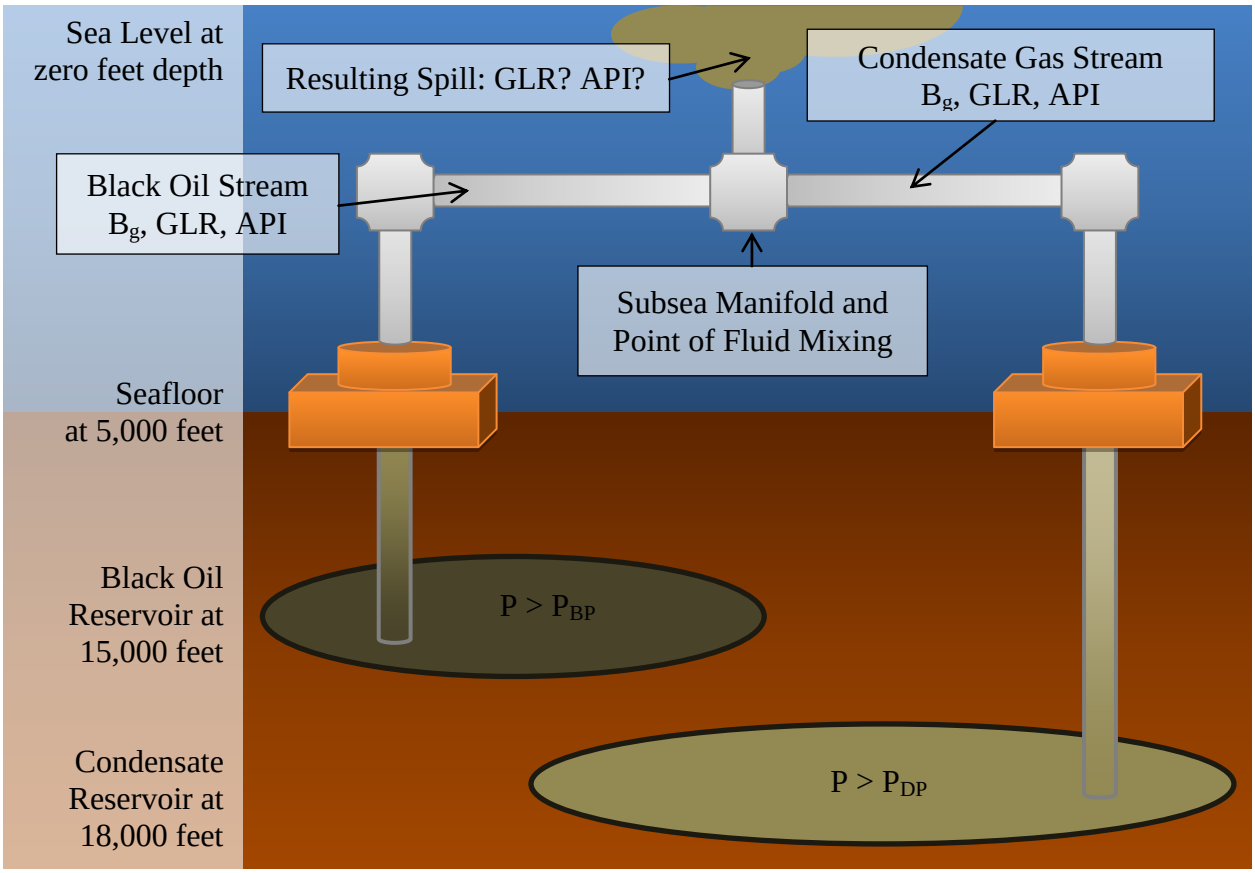

Figure 1. Schematic of the system, showing two reservoirs' fluids converging at simple T-joint on seafloor and downstream leak point.

This setup provides a look at contingencies which are becoming more realistic and probable as the frontier of deepwater drilling is expanded. The analysis of commingled flow through this junction is intriguing because it is the key difference between producing from a conventional offshore field versus one or more satellite fields.

2.2.1 Influence of Formation Parameters

Basic parameters, such as permeability and pressure, affect the inflow performance relationship (IPR). The concave downward appearance of an IPR curve (found by plotting wellbore flowing pressure against flow rate) expounds, amongst other things, the time-dependence of a well's productivity in a given reservoir (Walsh and Lake, 2003). However, on the time scale of a

blowout, one does not expect to see much change in reservoir pressure. Thus, a study of transient flow rates from a reservoir containing only liquid and lacking skin damage reveals the following results (seen in Figure 2). The natural flow point is indicated by the crossing of two curves, the IPR and the tubing performance relationship (TPR) curve, and predicts the maximum openhole flow for those conditions. The flowing bottomhole pressure (p_{wf}) is calculated by Equation 2.1 below (Walsh and Lake, 2003). There are actually many forms of this equation, but the one used to be consistent with the above assumptions and requirements is

$$p_{wf} = p_i - \frac{q_{osc}\mu_o B_o}{4\pi h_{res} K} \ln\left(\frac{4Kt}{e^{\gamma}\phi\mu_o c_t r_w^2}\right) \tag{2.1}$$

where K is permeability, h_{res} is reservoir thickness, p_i is initial reservoir pressure, μ_o is oil viscosity, t is time, γ is the Euler constant, ϕ is porosity, c_t is total isothermal compressibility, B_o is the oil formation volume factor and r_w is the radius of the well. Reservoir model 1 is the initial trial with properties listed in Table 1 (based on values from Millheim et al., 2011). Frontier fields, particularly those of Paleogene and Jurassic origin, are the target of this study as they pose the most challenges and risks. They differ from the conventional Pliocene and Miocene (commonly referred to as the Upper Tertiary) reservoirs in the Gulf of Mexico which currently account for almost 99% of proven reserves (Millheim et al., 2011). Aside from great water depths, reservoir complexity and quality are both problematic in comparison to the Upper Tertiary (Payne and Sandeen, 2013); high sulfur concentration is also another matter to contend with when safely operating these fields. Shell's Perdido platform produces from the Paleogene (and more specifically, Eocene-aged sands), which is known for having a high gas-oil ratio

(Millheim et al., 2011). Thus, it will be imperative to consider two phase flow, as it plays an important role in this study.

Table 1. Original Reservoir Properties Used in Sensitivity Study

Initial reservoir pressure	7,000 psia	Oil viscosity	5 cp
Permeability	100 mD	Formation volume factor	1.1
Porosity	20%	Total compressibility	10^{-6} psi^{-1}
Thickness	40 ft	Time	500 days
Reservoir radius	15,000 ft	Wellbore radius	4 inches

Lithology type is absent from the table above and can only be inferred from the porosity and permeability given. The pay thickness given is that of a massive bed and therefore does not include dual porosity modeling, which may be appropriate in other cases. This base reservoir model contains roughly 900 million stock tank barrels of oil initially. Also note that approximately one and a half years have elapsed from the first and only well being brought online; the inner diameter of the production tubing remains constant through out the well which contrasts with some tapered string designs currently in use and one of the examples to be reviewed later in Chapter 5. The remaining three reservoir models have single-parameter variations: permeability is reduced by a factor of ten in model 2, the porosity is divided by ten in reservoir model 3 and model 4's pay thickness is divided by ten. The greatest change seen in Figure 2 is the permeability reduction in model 2, which is an order of magnitude less permeable but maintains 70% of the oil rate. Model 3 nearly overlaps the original, showing only 0.6% reduction in oil flow rate and model 4 overlaps reservoir model 2 for a similar drop in flow rate.

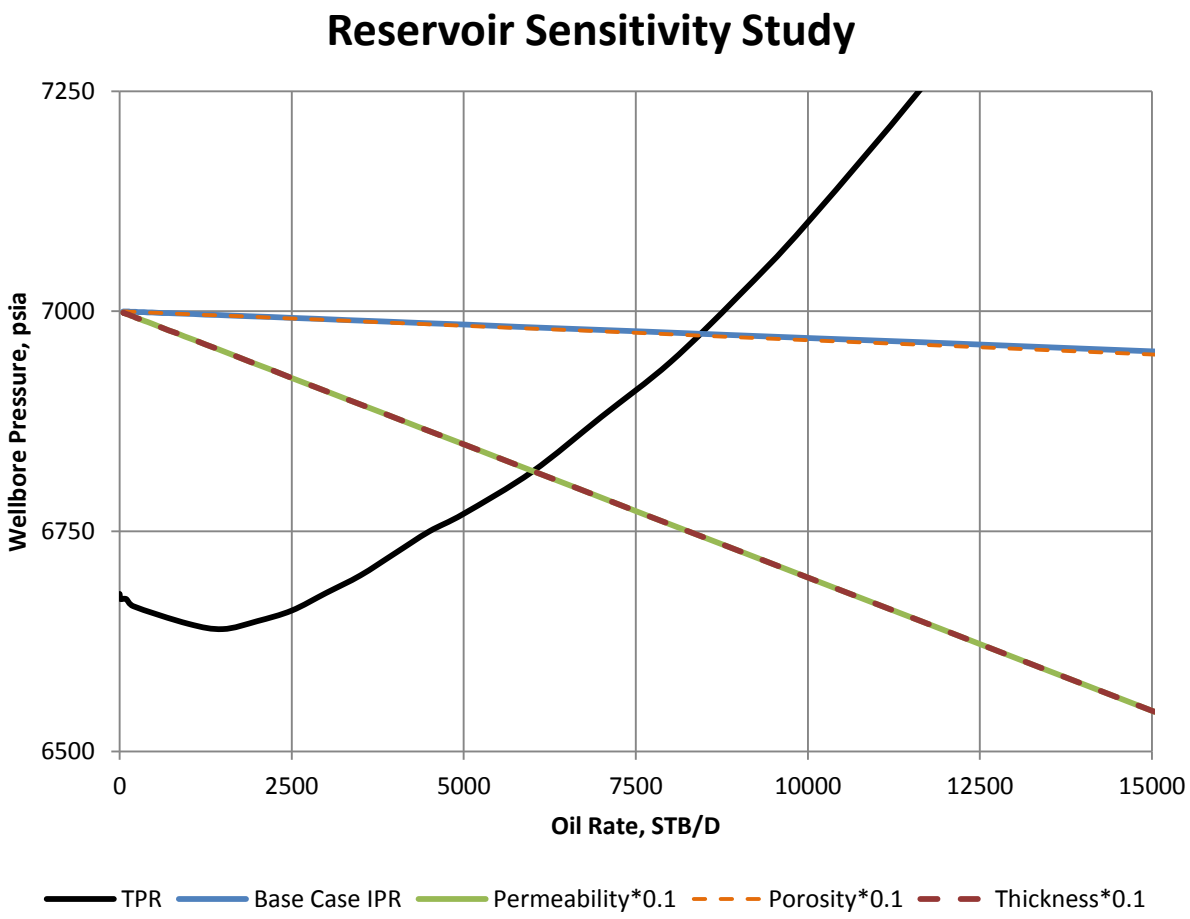

Figure 2. A Parametric Study of Reservoir Properties in a generic reservoir with three variations on its parameters shows how much the natural flow point of the system can change. The base case IPR results from the properties given exactly as in Table 1; the green curve represents model 2 with a permeability that is one tenth of the base case; porosity is reduced to only 20; and the final model's pay thickness has been reduced tenfold.

2.2.2 Fluid Properties and Flow Performance

Focus is now placed on the black oil fluid and how its characteristics can affect the flow rate and pressure drop within the system. A similar treatment is used in this investigation; namely, a base case is established and then each parameter is modified one at a time.

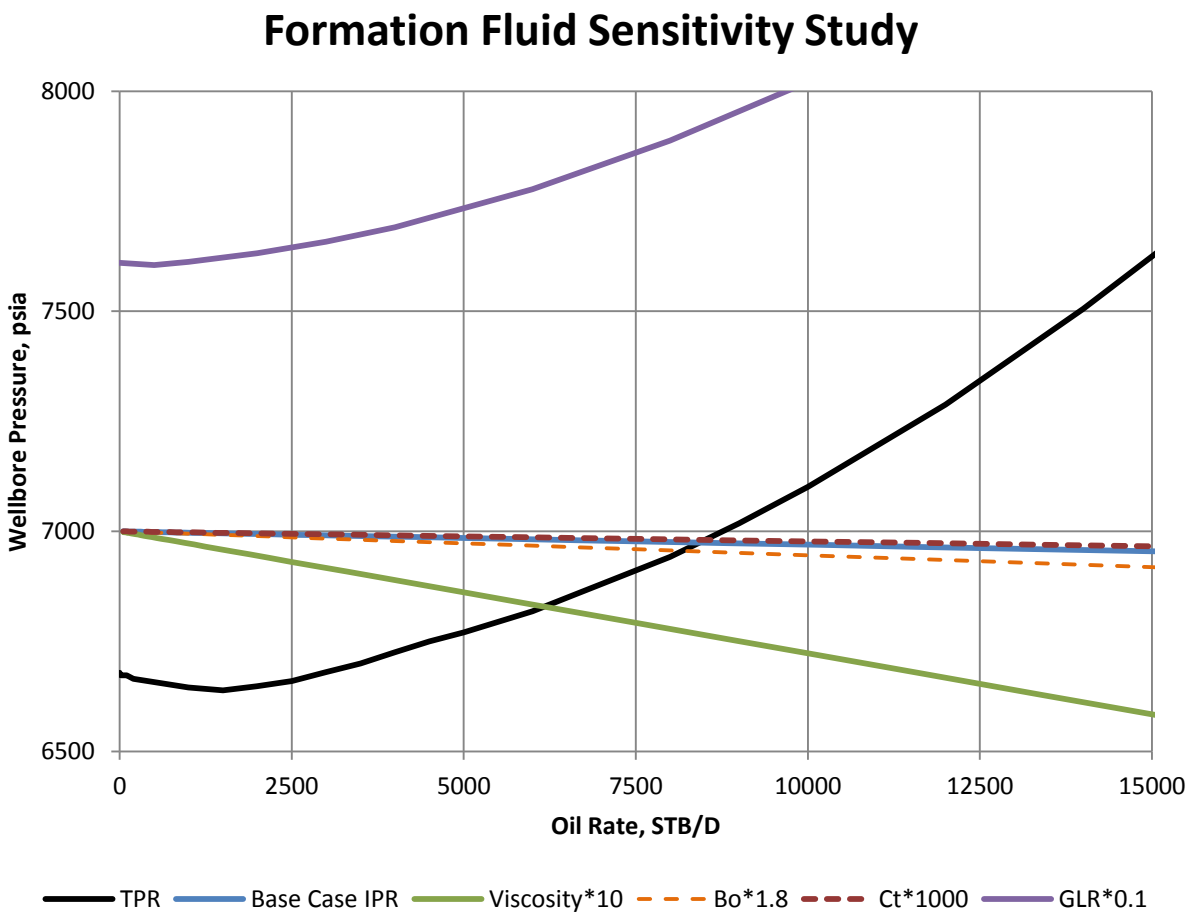

Figure 3. Comparing a generic reservoir model with four different fluids to show how the natural flow point of the system can change. The base case curve is the original IPR; the next IPR has an oil viscosity ten times greater than the base case; another case considered a formation volume factor 1.8 times larger, corresponding to 2.0; and total compressibility is tested at three magnitudes greater than the original. To assess the effects of gas-liquid ratios, a new TPR was generated which does not intersect at all with the IPR curves, thus indicating no flow.

A black oil, of 35 °API and a bubble point gas-oil ratio of 1,000 scf/bbl, is used for all the trials. Figure 3 displays the obvious result of gas-liquid ratio leading the parameters in influence on the reservoir's ability to flow; a tenfold decrease resulted in no-flow conditions. The next most important aspect is liquid viscosity, which drops flow rate by 27% after being multiplied by ten. Following far behind, B_o decreased flow by less than two percent when increased from 1.1 to 2.0

RB/STB and compressibility increased the produced flow by approximately 2.5% when multiplied by a thousand.

2.3 Impact of Production Tubing

Thirdly, the conduits used in the system are isolated to show that they have the greatest control over the pressure drop and, therefore, the relative phase rates present at the leak point. During the produced fluid's traverse, liquid will fall out and decrease what is known as liquid holdup (H_L) in the tubing (Hasan and Kabir, 2002). In addition to this, frictional pressure losses may liberate more vapors from the fluid, further decreasing H_L.

Changes in pressure loss with a myriad of tubing dimensions are discussed in Section 2.3.1. The dynamic nature of the gas-oil ratio (GOR) originating from one or both of the reservoirs will be the most intriguing aspect of the problem, because, as we just saw, it is a factor which impacts the rate of release at the leak point very strongly. Further evidence will be presented in Chapter 4. Pressure loss through the leak may lead to choked flow and will determine backpressure, which affects the TPR calculation in turn. Hence, an iterative process, as seen in Figure 4, will be required when simulating. A new technique, presented in Chapter 6, will shorten calculation time by bypassing nonessential steps, which are circled with dashed lines in the figure.

Langlinais (2013) incorporates several options for computing the TPR of a well containing at least two phases. An oil rate must be specified in order to run the Microsoft Excel VBA routine because the water rate and gas-liquid ratio are determined on that number. Other input required includes production tubing inner diameter, well depth (both measured and true vertical to capture behavior of deviated wells), fluid gravities, boundary conditions and desired correlations. The

latter consists of nine different models for various properties influencing the outcome of the tubing performance relationship curve.

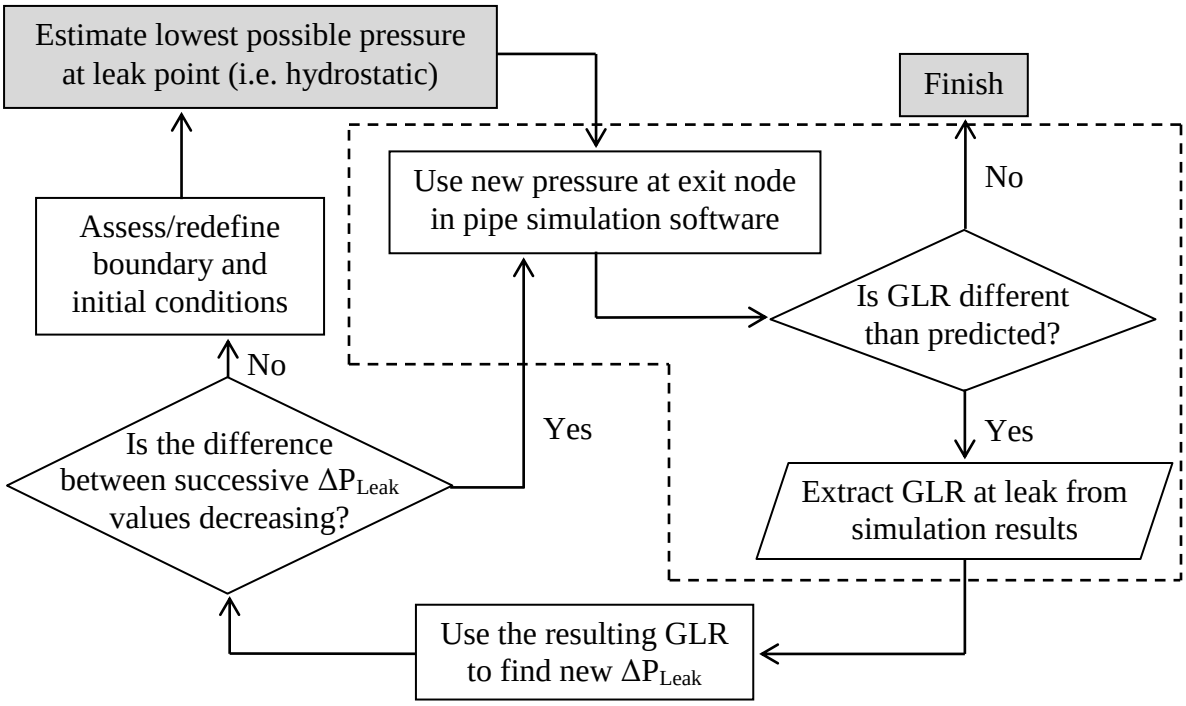

Figure 4. Start at the upper left with the process of estimating the leak point pressure. Follow through the diagram until a reasonably consistent prediction of GLR can be made, otherwise revise the system conditions and begin with the first block again.

2.3.1 Installed Components

Casing and production tubing are essential to ensuring a safe and efficient operation in the oil and gas business. They are also some of the most important items that engineers have complete control over during the design phase. As such, their properties should be fully understood not only to maximize production but also to use them safely.

The main point to be understood here is that a deeper condensate reservoir, at higher pressure, can have a great flow potential, but still contribute less to a mixture if removed far enough and constricted enough by a given well design. Well geometry is important in this regard, because

multiphase flow behaves differently for vertical and horizontal pipe (Duns and Ros, 1963). Drilling a deviated hole increases its measured depth (MD) and so it follows that extended reach wells will suffer greater pressure losses, since there was such a profound effect owing to increasing only the true vertical depth (TVD).

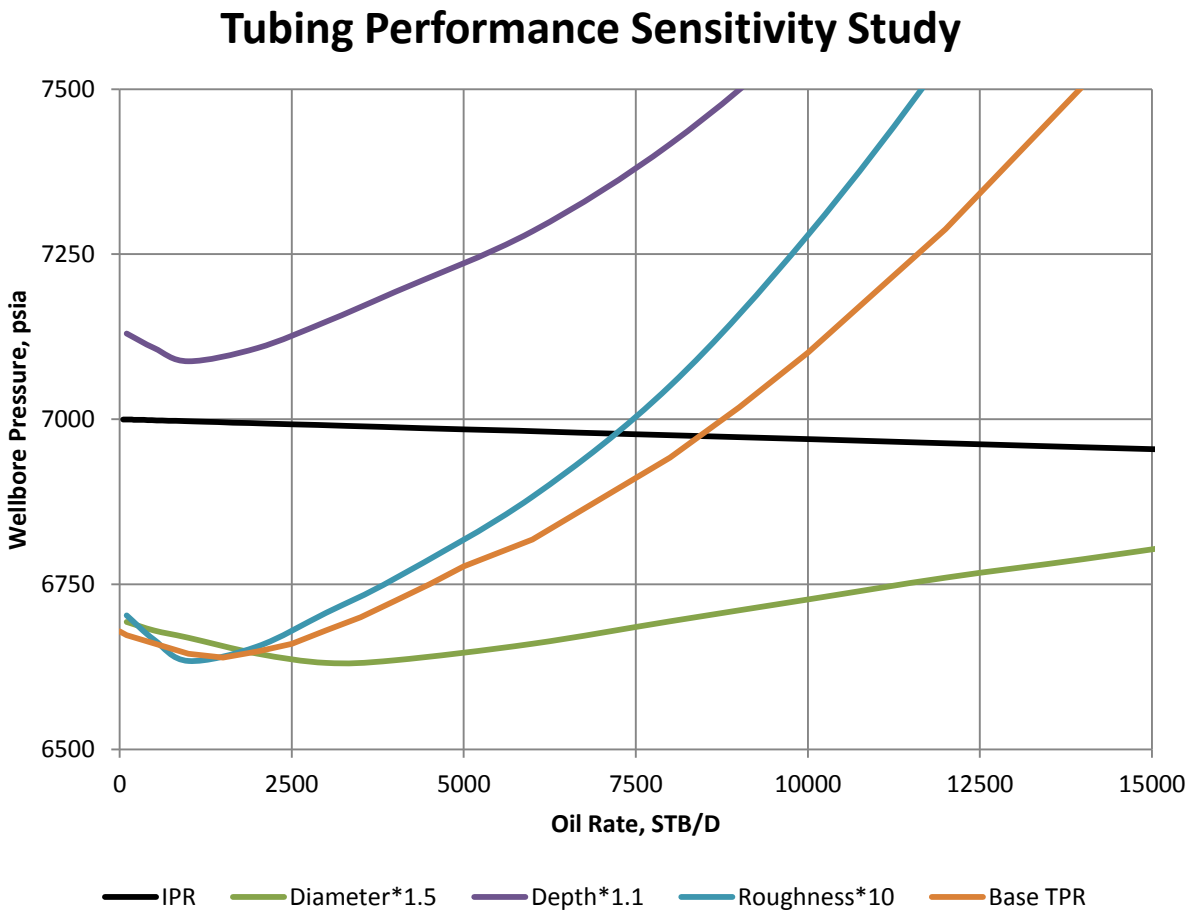

Figure 5. Contrasting different diameters, depths and various values of pipe roughness expose the strong influence of flow path in the well on absolute open flow. These flow potentials are quantified in Table 2.

Switching from a 3-inch pipe to a 4.5-inch pipe, both plausible sizes for offshore wells in the Gulf of Mexico, more than doubles daily rates. Also, within the range of the problem statement of 15,000 and 18,000 feet of true vertical depth, there is an increase of about 170% flow rate as

seen in Table 2. These two elements alone make for a variable system, especially if the fluid is lighter and its composition engenders two phases as it nears the sea floor (volatile oil and definitely retrograde condensates).

Table 2. Results of TPR Sensitivity Study

TPR	Modification	Flow Potential (BOPD)	Change
1	Original case	8,410	-
2	Diameter increased 50%	22,650	+169.3%
3	Depth increased 10%	0	-100%
4	Pipe roughness increased tenfold	7,215	-14.2%

2.3.2 Geometry of Tubulars

Though the engineer can detail the exact specifications of tubulars used in a well, one may not always have ideal profiles to work with. Horizontal wells exemplify this point clearly insofar as they can be toe-up (where the bottom of the hole is not the deepest portion of the well), toe-down (the bottom of the well is lower than the heel, below the kick-off point, of the well) or somewhere in between. A toe-up configuration carries the obvious consequence of loading up the heel of the well with liquid hydrocarbon or water, thereby reducing the productive capabilities of the well. Since the immediate concern of this study is to analyze worst case scenarios, these wells will not be given thorough treatment.

2.4 Preliminary Conclusions from Performance Relationships

Examination of each portion of the system in a blowout reveals that it is tubing constrained. Neither geology nor formation fluid has as strong an influence on production as the conduits used, according to Duns and Ros (1963), who break down pressure losses in hydrocarbon

production. They state that tubing is responsible for between 57% and 82% of the pressure loss in petroleum systems, followed by the reservoir which accounts for 11% to 36% of losses. The remainder of the pressure losses in the system is found in the surface lines (typically amounting to no more than 7%). These findings are graphically represented in Figure 6 to emphasize the lesser significance of reservoir properties and the stronger influence of GOR.

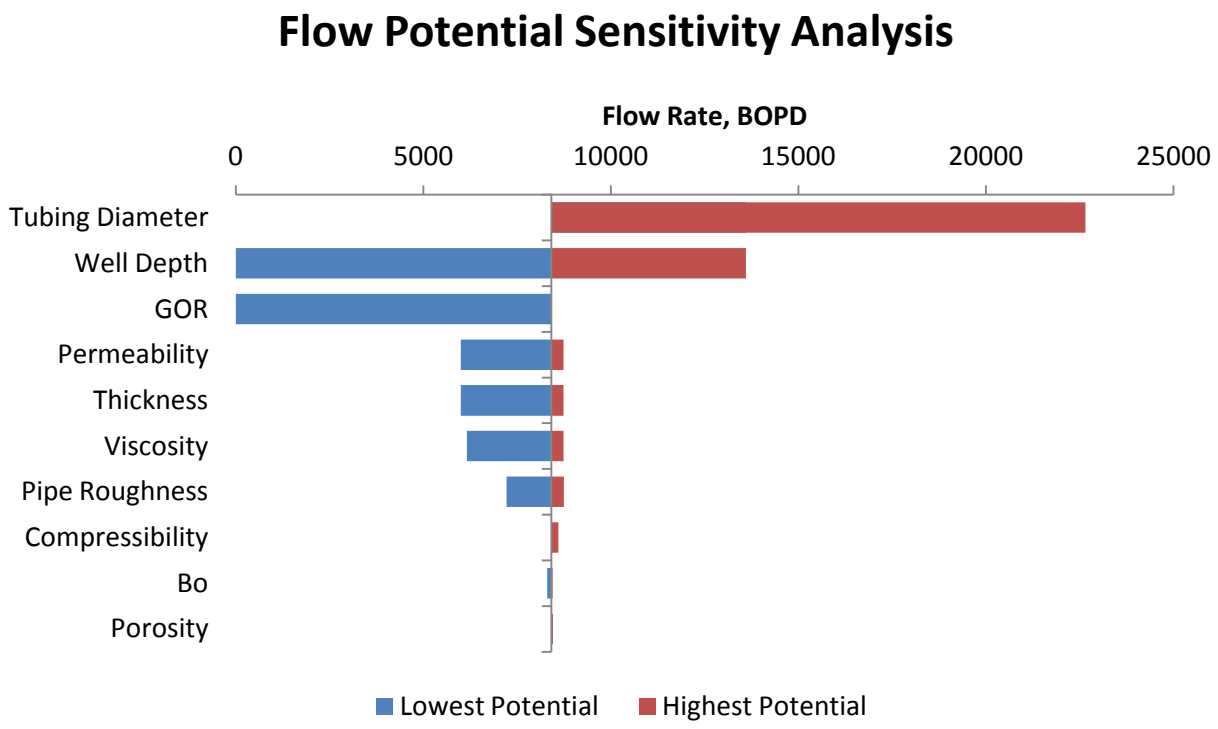

Figure 6. This overview of governing variables in hydrocarbon production illustrates the skewed level of importance away from reservoir properties and towards well properties and GOR.

The tornado chart above shows the difference in surface flow rates under the various circumstances explored in this chapter. The base case of 8,410 barrels per day is identified by the vertical axis, which divides the flow rate potentials between the lowest possible and the highest reasonable. In other words, porosity was reduced by one order of magnitude (to 2% porosity) for the smallest flow rate and adjusted to 100% for the highest as an entire order of magnitude

greater (namely, 200% porosity) does not make physical sense. The other parameters were handled similarly, with either practical values or one order magnitude being the constraint. Tubing diameter far outstrips other variables with a spread of approximately 19,400 barrels of oil per day (BOPD), followed by the well depth varying the possible flow rate by 13,600 BOPD and then GOR giving a range of 8,400 BOPD.

An argument could be made that some of these variables have the potential to vary more than just one order of magnitude, such as permeability which can be measured, in currently producing reservoirs, in nanodarcys (Iwere et al., 2012) to darcys. Again, the comparison provided here is limited to what is encountered in the deeper waters of the Gulf of Mexico and thus the base properties are similar to those encountered in the Lower Tertiary and Jurassic formations.

Chapter 3
Theory of Implemented Tools

3.1 Nodal Analysis

Now a standard engineering tool for production facilities and well planning, nodal analysis studies two sets of parameters typically grouped within either the inflow or outflow section of a system (Hein, 1987). Gilbert (1954) proposed this method for the optimization of wells on artificial lift, but it took some time until industry adopted it in earnest. Mach et al. (1979) took up the mantle of nodal analysis and originally defined eight different nodes, with two additional depending on the level of detail for surface equipment; however, the number of nodes can be reduced to four by segmenting the system at the inflow point (reservoir pressure, $\overline{P}_r$), the bottomhole (P_{wf}), the wellhead (P_{wh}), and finally the separator (P_{sep}). This approach remains an effective teaching tool, but lacks the intricacy of a numerical simulator such as SPT Group's Oil and Gas Simulator (formally known as OLGA®). The complexity of fluid behavior is also lost without proper modeling with an equation of state, now typically handled by computer programs like PVTsim® from Calsep.

3.2 Simulation Software Packages OLGA® and PVTsim®

Production flow simulators have been under development for decades by authors such as Bendiksen, Malnes, Moe, and Nuland from the Institute for Energy Technology (IFE), as well as Viggiani, Mariani, Battarra, Annunziato, and Bollettini of the Pipeline Simulation Interest Group (PSIG). A maximum of two phases was allowed by the simulator OLGA®®, which saw its first operable version release in the early 1980s. It did not realize its full potential until a joint venture of several companies (Conoco Norway, Esso Norge, Mobil Exploration Norway, Norsk Hydro

A/S, Petro Canada, Saga Petroleum, Statoil and Texaco Exploration Norway under the SINTEF banner) pooled their resources (Bendiksen, 1991). This development brought together several empirical correlations into a single system. It still relies upon flow regime maps, but integrates them with a more concrete understanding of physics. One organization of regimes, provided in Figure 7, shows how Duns and Ros (1963) defined vertical two-phase flow.

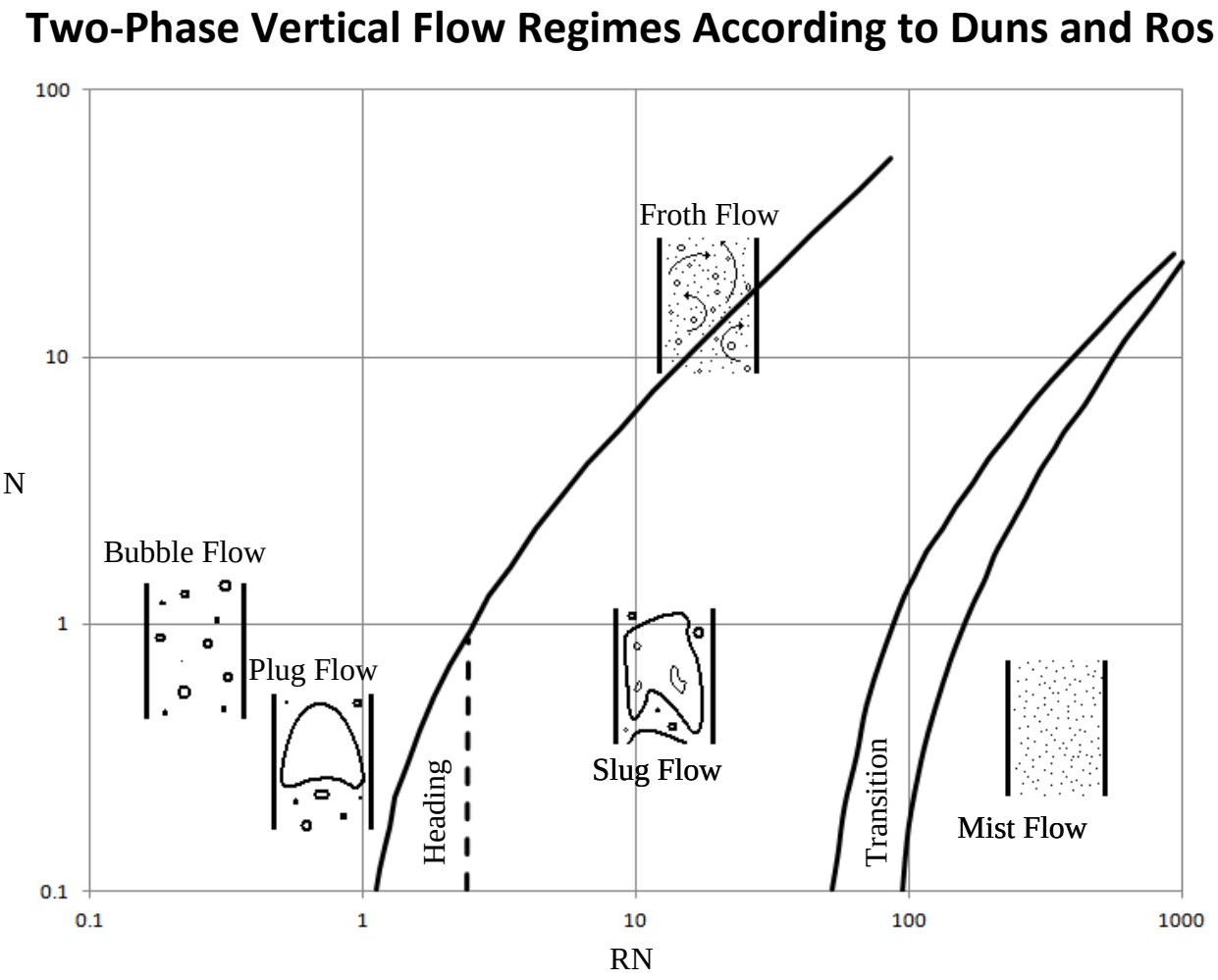

Figure 7. Flow pattern map, after Duns and Ros (1963), defines regions of fluid flow for which appropriate frictional loss correlations should be used.

The dimensionless liquid velocity number, *N*, and dimensionless gas velocity number, *RN*, are defined by equations 3.1 and 3.2, respectively. These governing groups take into account the

superficial velocity, v_s, liquid density, ρ_l, gravity, g, and the interfacial tension, σ, between the two phases present.

$$N = v_{sl} \sqrt[4]{\rho_l / g\sigma} \tag{3.1}$$

$$RN = v_{sg} \sqrt[4]{\rho_l / g\sigma} \tag{3.2}$$

It is important to note that these numbers were established in a study that dealt with mixtures of oil and gas with no water present. Interfacial tension is incorporated in both numbers to allow the use of the Duns and Ros (1963) method with low concentrations of water, however the formation of stable oil-water emulsions causes the correlation to break down when predicting frictional pressure losses in vertical flow. Pressure losses in water and gas mixtures can also be assessed with practical (Duns and Ros, 1963) accuracy, but will not yield comparable results to those of oil-gas systems. Thus, it is safe to use these groups in the present deepwater system as the flowing pressure at the leak will generally exceed hydrostatic pressure.

3.2.1 The Flow Assurance Software OLGA®

OLGA® divides flow types into two regimes: separated flow and distributed flow. The former contains stratified and annular flow behavior, while the latter describes dispersed bubble flow and hydrodynamic slug flow. The most important metric for determining which of these exists is the slip, which is a ratio of average gas velocity to average liquid velocity (OLGA®, 2012). Once determined, this information can be fed into a system of equations (ranging from a few equations for a simple system to seven or more) for a one-dimensional simulation; typically though, five mass conservation equations, three momentum equations and one energy conservation equation

are coupled with transfer equations in the dynamic three-phase flow simulations computed by OLGA® (Anderson, 2012). All of these are limited spatially and by time step according to the accuracy required and the Courant number (also known as the Courant, Friedrichs and Lewy number or CFL). A general guideline for node lengths (Δx_i) is given in the OLGA® user manual (2012) and represented in equation 3.3 below; it concerns the accuracy of the representation of the partial differential equation being solved.

$$\frac{1}{2} \leq \frac{\Delta x_i}{\Delta x_{i+1}} \leq 2 \tag{3.3}$$

This also implies that each pipe should have at least two sections, but the likelihood is that pipes will have several sections to honor the profile of a well or topography of a pipeline network. This discussion on numerical stability and accuracy is important to the modeling of the choke in OLGA® (see Figure 11 in Chapter 4 for the cross-section investigated). Courant, Friedrichs and Lewy determined that the step size of the spatial and temporal variables in the numerical solution of a partial differential equation control the stability of the finite-difference representation of the physical system (Courant et al., 1967 and Tannehill et al., 1997). This is visualized in Figure 8 with an invalid and valid example using the velocity of a particle inside a conduit.

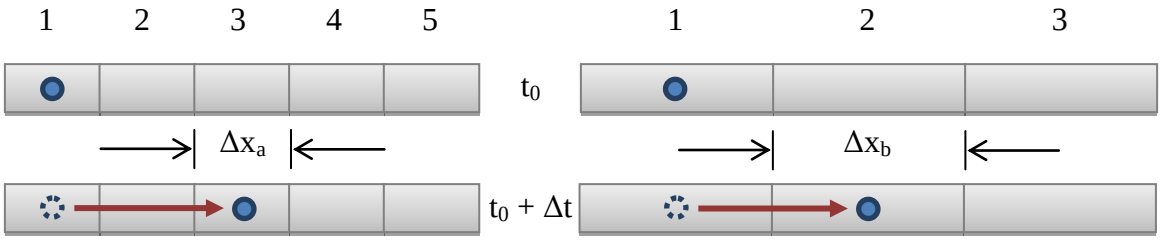

Figure 8. The Courant number ensures stability within this explicit time marching scheme. Both simulations use the same time step (Δt), but the gridding of pipe *a* is too fine. A fluid particle may travel further than the resolution (Δx_a) in this case, whereas Δx_b is properly sized to preclude numerical instability in the simulation.

Trefethen (1996) mentions that the amount of time progressed per step must be short enough so that no spatial discretization is skipped during computation.

$$C = \frac{u\Delta t}{\Delta x} \leq C_{\max} \tag{3.4}$$

It should also be noted that the approach to numerically integrating flow is decoupled vis-à-vis temperature, which normally contributes a ±15% error (OLGA®, 2012); there is a hard-coded correction built into the software to address this issue. Thermal considerations are minimal in this work as the fluids flow quickly through the pipe to the seafloor and are therefore subject to little heat loss until passing through the leak.

Boundary conditions required by the program include temperature, GLR, and pressure or flow rate at inlets and outlets. The temperature and pressure are crucial as a number of intensive properties are computed with them. PVTsim®, the phase behavior software discussed in the next section, supplies tabulated information on the fluids to be used in the simulation; any value not present in the simulation data file is interpolated from the tabulated information. Concerning rheology, OLGA® assumes the flowing fluids to be Newtonian for basic calculations and uses empirical correlations, available in sub-modules, to handle non-Newtonian fluids. The manner in which a liquid or gas behaves at turns, bends and other obstructions must be approximated through coefficients by the user. Improvements on these discharge coefficients may be obtainable from detailed computational fluid dynamic (CFD) studies.

3.2.2 Phase Behavior and PVTsim®

J.D. van der Waals proposed an equation of state in 1873 to reflect the behavior of real fluids, specifically the attraction between their constituent molecules and the volume each molecule

occupies (McCain, 1990). However, this equation is valid only at low pressures, which restricts its application mainly to liquids and low-pressure gases (McCain, 1990). Equation 3.3 expresses the van der Waals relationship in cubic form.

$$V_M^3 - \left(b + \frac{RT}{p}\right)V_M^2 + \left(\frac{a}{p}\right)V_M - \frac{ab}{p} = 0 \tag{3.5}$$

Attractive forces are denoted by the constant *a* which corrects for pressure by an amount of a/V_M^2 when added to an unadjusted system pressure. The volume occupied by molecules is introduced via the constant *b*; both *a* and *b* are specific to a given fluid. The term V_M is molar volume and *R* represents the universal gas constant in whichever form is appropriate to the units being used. A host of equations of state followed in this vein, but, according to McCain (1990), the most noteworthy came from Redlich and Kwong in 1949 (with a modification later offered by Soave in 1972) and Peng and Robinson in 1976. These are known as the SRK and PR equations of state, respectively. Peneloux et al. (1982) stated that the SRK equation of state gives reasonable results for pure components with low values for the acentric factor, like methane. They refined the SRK expression with a volume correcting constant, which enhances the predictions of liquid density at the cost of requiring another fluid parameter beyond critical properties and the acentric factor (Riazi and Mansoori, 1992). PVTsim® provides the option of using either the SRK or the PR equation of state with the static or temperature-dependent version of the Peneloux volume correction, often denoted by the letter *c*. In the present study, the SRK equation of state is used with the Peneloux correction.

Mixing is of primary interest in the current study, an explanation of the insufficiency of classical mixing rules is required. Water is a polar molecule and when paired with one other nonpolar

component (such as any hydrocarbon), the classical mixing rules fail to provide a reasonable value for attractive forces, the *a* parameter (PVTsim®, 2012). This disparity in charge tends to layer by component type (i.e. alternating polar and nonpolar zones of molecules) and therefore create a structure in the mixture (Pedersen and Milter, 2004). By default, the Huron and Vidal (H&V) rule of 1979 is employed to combat this situation in scenarios involving not only water, but salts and hydrate inhibitors (PVTsim®, 2012). High pressure, high temperature cases are of particular interest in this study since deepwater wells typically have both elevated reservoir pressures and reservoir temperatures. Pedersen and Milter (2004) surveyed the effectiveness of the H&V correction and the Cubic Plus Association (CPA) model when applied to gas condensates, which have a significant amount of gas in the water phase. The variations incorporated in these schemes need not be applied universally; most binary interaction parameters (hydrocarbon-hydrocarbon pairs namely) can be calculated with the classical mixing rule while others involving water, methanol, and others can be treated by the H&V or CPA exception. Within the 35°C to 200°C range and 700 bar to 1000 bar window, the predictions using H&V proved satisfactory.

Simulating multiple phases requires that fugacity, or effective pressure, be considered. Accurately describing PVT behavior for a gas that is real requires the matching of its chemical potential at a specified temperature and pressure with an ideal gas at the same temperature, but different pressure. Although this chemical potential, or partial molar free energy, is not typically expended during normal (non-flaring) production or blowouts, it does relate to phase changes (Job and Herrmann, 2006) that often occur between bottomhole conditions and manifolds or platforms. In the presence of equilibrated vapor and liquid, fugacity and chemical potential are equal in both phases. The general expression of fugacity is

$$\ln \varphi_i = \frac{-1}{RT} \int_{\infty}^{V} \left(\left(\frac{\partial P}{\partial n_i} \right)_{T,V,n} - \frac{RT}{V} \right) dV - \ln Z \tag{3.6}$$

where n_i represents the moles of component i and Z is the compressibility factor (PVTsim®, 2012). The use of fugacity allows for better accuracy in predicting equilibrium at greater pressures, which will be encountered in any oil or gas well. Once two phases equilibrate then the composition for each can be calculated. Thus, the relative amounts of each phase and their physical properties used in flow calculations can be generated. These calculations must be made along the entire flow path of each reservoir fluid in this study, because a great deal of change can occur in the fluids before they interact with each other. The literature and software available now adequately predict these changes up until the point of mixing.

PVTsim® incorporates a mixing scheme called *allocation* after the process that Pedersen (2005) describes. The module requires molar composition of each feed stream, each stream's volumetric flow rate at specific pressure and temperature, and the "process plant" configuration in order to compute the contributions provided from all sources. To do so, PVTsim® breaks down the composition of each fluid into common discrete components and pseudocomponents. Those components deemed necessary are created on the basis of mass flow rate entering the process plant. Converting the volumetric rates to molar rates is accomplished assuming complete mixing for the given pressure and temperature given. The results of these allocation computations often do no better than other means of simulating as Chapter 6 describes. This study picks up here and establishes a similar process based upon flow rates, but only using the heptanes-plus pseudocomponent in the correlation. Again, the focus is producing consistent gas-oil ratios for use in flow rate equations where information is limited.

Chapter 4
Leak Geometry and Discharge Coefficient

Before discussing the tools and processes used in this study, the leak itself must be described in finer detail. So far the leak has been regarded as an arbitrary back pressure on a system of converging well streams. This is essentially true, but calculating that resistance to flow becomes a challenge when considering the types of leaks possible in deep water operations. Nichol and Kariyawasam (2000) analyzed the risks associated with neglecting wells and, even though the present study does not assume wells to be temporarily abandoned or shut-in, the failure mode analysis provides insight on weak points in offshore production.

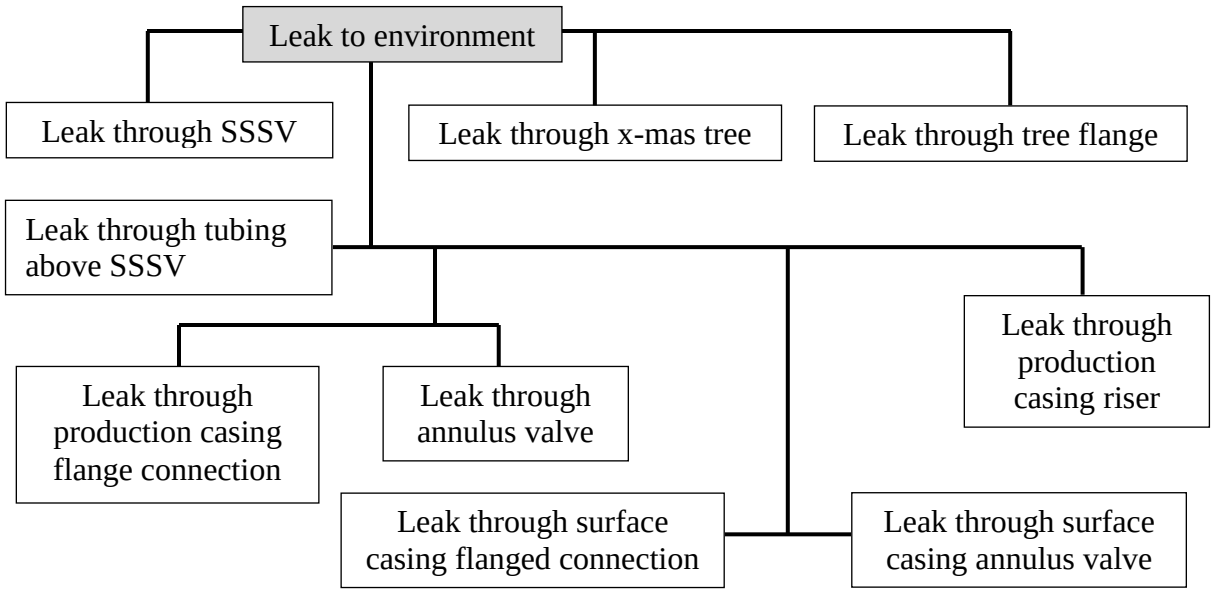

Figure 9. The final consequence of a blowout is located at the top of this failure mode tree with some possible fault mechanisms listed in the branches beneath it.

The type of leak geometry can vary depending on the cause described in Figure 9 and any backup safety measures downstream of the leak. The items closest to the top are nearer to the spill and are likely to have leaks of greater area and thus higher flow directly to the seafloor.

4.1 Sheared or Parted Pipe

Perhaps the worst case scenario for a subsea blowout is when a conduit, whether it is production tubing or seafloor flow lines, breaks open entirely. Hurricanes can generate tremendous force, which break sediment loose near production platforms, ultimately resulting in mudslides. When hurricane Camille hit the Gulf of Mexico with nearly 70-foot high waves in 1969, such deformation occurred in the South Pass Block 70. One platform was destroyed entirely and another experienced a great deal of damage (Nodine et al., 2006).

4.1.1 Gilbert Discharge Equation

The risk of shearing a pipe in this fashion will not be an issue in deep waters, but other ruptures exposing the full diameter of a flow line would certainly cause the greatest amount of environmental damage. This type of leak has been discussed at length in the literature and one of the most enduring models for such a scenario was initially proposed by Gilbert (1954).

$$Q_L = \frac{P \cdot d_{64}^A}{B \cdot GOR^C} \tag{4.1}$$

The liquid rate, Q_L, is estimated with pressure, P, the opening diameter, d_{64}, and the gas-oil ratio. The constants A, B and C are the subject of several papers as seen in Table 3.

Table 3. Coefficients Proposed for the Gilbert Flow Equation.

	Coefficients		
Correlation Author	**A**	**B**	**C**
Gilbert (1954)	1.89	10.01	0.546
Baxendell (1957)	1.93	9.56	0.546
Ros (1959)	2	17.4	0.5
Pilehvari (1980)	2.11	46.67	0.313

Equation 4.1 is attractive because of its ease of use; the pressure can be estimated at hydrostatic, the inner diameter of the burst pipe is known and the GOR is known for each well stream contributing to the leak. The way these GORs combine is left for a later discussion in the results, but may be correlated to give an approximation of flow using Gilbert's correlation.

However, a number of limitations exist on this correlation, because it was developed for a specific oilfield and set of pipe and valve diameters. Gilbert (1954) sampled the Ten Section Field in the San Joaquin Valley in Kern County, California. It was this context that provided the tubing size to be no more than 3 ½ inches inner diameter, the GLR is between 2,000 and 500,000 scf/stb, API gravity of 25-40 degrees for the oil and an upper limit of an inch for the bean (a colloquialism for orifice) size. The relationship was initially intended to aid gas-lift design for the area, which was the first production in the valley after seismic surveys discovered the potential in the 1930s (Lietz, 1949). It is understood that this tool is meant for mature onshore fields, but should apply equally well to the case presented herein if the above parameters are kept within a reasonable range of the correlation and that the flow through the leak is choked.

4.1.2 Validity of the Gilbert Equation and Other Methods for Seafloor Leaks

To ensure that Equation 4.1 is applicable to the present study, data is collected from Ashford (1974) and reproduced with new calculations in Figure 10 and Table 4. In Gilbert's study (1954), it is assumed that flow through the bean is supersonic and that upstream pressure is at least 70% greater than pressure downstream of the restriction (thereby ensuring choked flow).

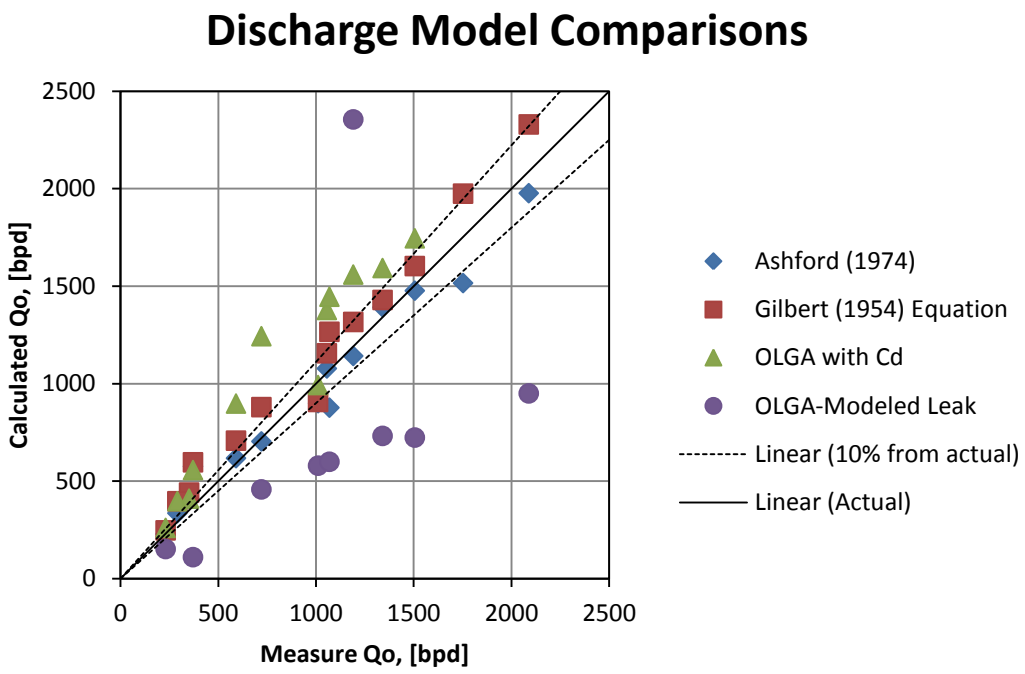

Figure 10. Existing models from the literature are tested against a data set from Ashford (1974) to confirm their validity next to the OLGA® models being considered.

Table 4. Relative Differences of Various Discharge Estimation Methods

Well	d_{64}	R	P_1	T_1	γ_{oil}	Measured Q_o	Ashford	Gilbert & Baxendell	OLGA® model	OLGA® with C_D
(-)	(-)	(scf/STB)	(psia)	(°F)	(H_2O=1)	(bbl/D)	(%)	(%)	(%)	(%)
1	32	1065	485	120	0.844	1010	-10.89	-10.26	-42.62	-1.69
	16	1065	505	120	0.844	230	-0.43	7.68	-33.91	13.29
2	32	180	325	120	0.885	1505	-1.86	6.52	-51.91	15.99
	24	180	465	120	0.885	1190	-4.03	10.63	97.92	31.07
	16	173	665	120	0.885	720	-2.22	22.18	-36.41	72.72
3	32	363	425	120	0.867	1340	3.88	6.67	-45.36	18.88
	24	337	575	120	0.867	1055	2.18	9.57	1579.54	30.61
	16	341	775	120	0.867	590	4.75	19.97	2797.80	52.22
4	32	118	375	120	0.883	2088	-5.32	11.57	-54.49	108.23
	24	107	525	120	0.883	1752	-13.47	12.70	1212.39	57.09
	16	108	740	120	0.883	1068	-17.88	18.55	-43.87	35.38
5	32	127	100	120	0.882	370	55.68	61.29	-70.16	50.53
	24	120	125	120	0.882	350	17.71	26.17	1722.94	17.26
	16	102	225	120	0.882	290	15.86	36.96	2127.63	36.99

Ros (1961) describes critical flow criterion through a choke simply when the ratio of downstream pressure to upstream pressure is 0.544. Extrapolating this to systems with different parameters creates errors, which can be mitigated through the use of discharge coefficients (C_D) according to Ashford (1974). This term is incorporated to absorb irreversible losses not predicted by the Bernoulli equation (Ajienka et al., 1994, Rahman et al., 2009). The calculations from Ashford (1974) in Table 4 use values for C_D ranging between 0.642 and 1.218 from the process outlined in the same paper. To perform this calculation, the Z-factor must first be evaluated from lab measurements as reasonably as possible (gas composition can be erratic and cause problems in some instances, so an average may be necessary). Inserting this number into Equation 4.2 allows the liquid flow rate to be calculated. The resulting flow rate is, of course, theoretical and must be compared to the actual rate observed; their difference, in the ratio form of q_L-measured to q_L-predicted, will be the discharge coefficient.

$$Q_L = 1.53 \frac{d_{64}^2 p_1}{\left(B_o + F_{wo}\right)^{1/2}} \times \frac{\left\{\left[T_1 Z_1 (R - R_S) + 151\rho_1\right]\left(SG_L + 0.000217 SG_g R_S + F_{wo} SG_{wo}\right)\right\}^{1/2}}{\left[T_1 Z_1 (R - R_S) + 111\rho_1\right]\left(SG_L + 0.000217 SG_g R + F_{wo} SG_{wo}\right)} \qquad (4.2)$$

All quantities used are measured in field units. The complexity of Equation 4.2 is reduced considerably by removing the water-oil ratio (F_{wo}) for cases not involving water. *SG* denotes the specific gravity, whether it be for the liquid, vapor or water phase. All other definitions remain the same as previously described or industry-accepted, such as the gas compressibility (*Z*), gas-oil ratio (*R*) and solution gas-oil ratio (R_S). Again, the C_D is a ratio (refer to Equation 4.3) of the measured to calculated and thus expected to be less than unity.

$$C_D = \frac{Q_{L,measured}}{Q_{L,predicted}} \qquad (4.3)$$

The "Gilbert & Baxendell" column contains results from Equation 4.1 using the Baxendell coefficients. The simulation software OLGA®, to be discussed in more detail within Chapter 5, is used to predict flow in two ways. The first, "OLGA®-model," describes a conduit that tapers down to the size of the orifice being studied. Simulating abrupt changes in pipe diameter is difficult, because it creates problems when the software's solving routine attempts to converge on a solution. A 16/64" venturi-style choke is modeled in OLGA® in a manner as seen in Figure 11. However, OLGA® can also use correlations with a suggested (but changeable) C_D of 0.84 to provide much more accurate results. As mentioned before, Ashford (1974) used several values of C_D while the "OLGA® with C_D" model uses only the default discharge coefficient. The C_D works best in the ½-inch case (three out of the five scenarios) and suggests a lower value for smaller chokes.

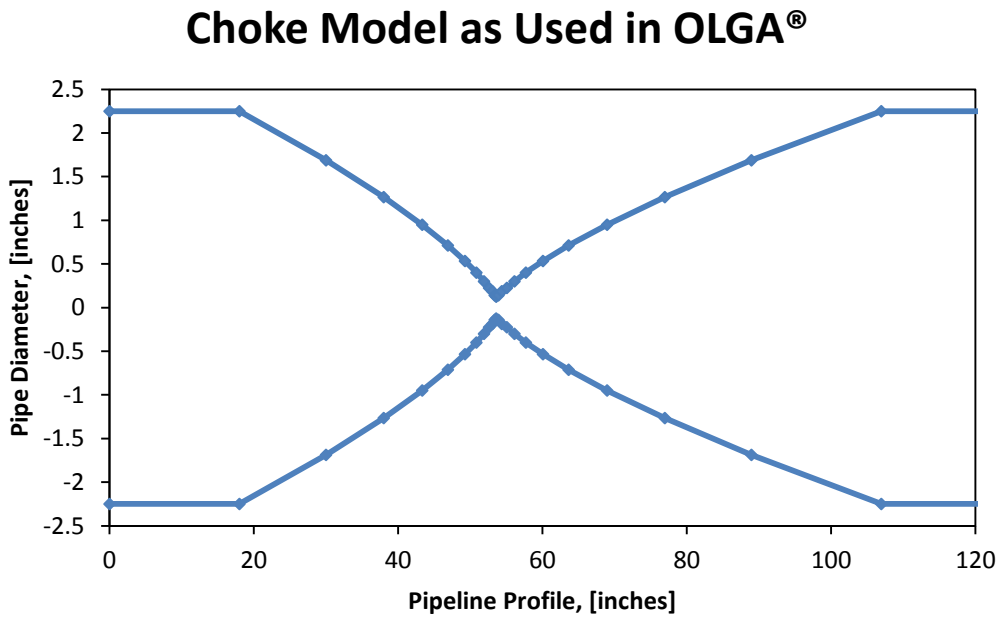

Figure 11. The pipe geometry in OLGA® must be tapered gradually to prevent the software from crashing during simulation runs. This results in very erroneous results and provides the motivation to further study leaks with a proper CFD package that analyzes three dimensions.

4.2 Leaking from a Failed Flange Connection

Another type of leak geometry that could be encountered is around the wellhead or where any pipes mate with the aid of flanges. There are different types of connections with advantages and disadvantages for the kind of element used between flange faces. In a basic flange, a groove is cut into the face of the flange with a particular profile wherein a gasket sits. Reusable types of gaskets are typically made of rubber, but they do not provide adequate containment for high pressure fluids. Metal gaskets, or O-rings as they are sometimes called, can seal at higher temperatures and pressures than rubber counterparts. However, the metal rings actually deform during the process of tightening the flange bolts to provide the stronger seal, so they cannot be used more than once. The failure of either ring can, of course, vary between a trickle to completely eroded rings where fluid can escape via the flange-face grooves.

Deep water wells are considerably more complex than implied by the wellhead schematic in Figure 12. However, the diagram underlines the importance of the gasket that completes the flange connection since these flange connections are used throughout the subsea equipment (see Figure 13) as well as the well casings. Figure 12 shows how it may come under the influence of two different zones in the case of bad cement jobs or other minute leak paths.

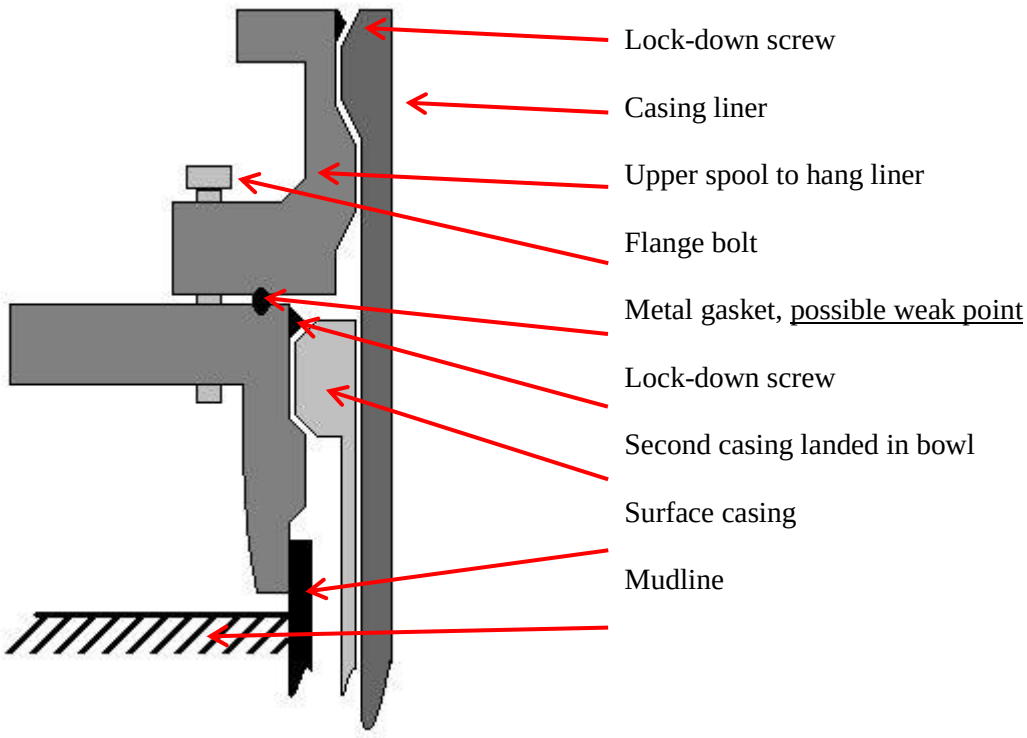

Figure 12. This cross-section of a typical wellhead details common components and highlights the gasket as the most plausible location of failure. The surface casing is likely not to fail where it is connected to the lower flange, because it is welded (joint not explicitly shown).

Figure 13. Well containment warehouses are being stocked so emergency responders can react to blowouts with the right equipment in a timely fashion. Depending on the function and pressure rating, flanges may have a few thick bolts or several of them evenly spaced out. Photographs were taken by Muhammad Zulqarnain while on tour at the Marine Well Containment Company's facility in Houston, Texas.

4.3 Arbitrary Hole Shape and Modifications to the Flow Equation

In the case of parted tubing, an irregular hole may manifest and create complex fluid paths for hydrocarbon spills. After rearranging Equation 4.1 to isolate pressure, a discharge coefficient can be applied in order to adapt the Gilbert equation to reflect the nature of the leak. Figure 14 displays a generic conduit with an oddly shaped hole in the side. Dotted lines partition the leak off by flow behavior: the *N* denotes for nozzle and infers a jetting action as fluids are accelerated through the narrower opening and the *D* stands for diffuser because these areas are likely to see a slower velocity as fluid has relatively more freedom to expand in these sections. If partitioned properly, then each of these zones could be calculated separately with their own discharge coefficient. Compiling the results of these sections afterward could potentially improve the results of Equation 4.1 and overall simulations in software such as OLGA®. The importance of these discharge coefficients can be seen in Table 5, which shows liquid discharge within several cases. These trials were run in OLGA® using the proper discharge coefficient for each bean size (and not attempting to specifically model the choke within the geometry editor) to find the liquid flow rate through a 3 ½" pipe and then Equation 4.1 was used to predict these same rates.

Table 5. Liquid Rates (MBPD) Resulting from Different Pressures and Gas-Liquid Ratios

		OLGA®	**Gilbert**	**OLGA®**	**Gilbert**	**OLGA®**	**Gilbert**
GOR	4,000 scf/stb	29	14	19	22	38	35
	1,000 scf/stb	36	21	41	44	51	56
	500 scf/stb	38	30	45	36	57	79
		Noncritical Flow		Sonic Flow		Sonic Flow	
		3,500 psia		4,000 psia		5,000 psia	
		Upstream Pressure					

Fluid flow was constrained in these trials by first holding upstream pressure constant and varying the gas-oil ratio and then increasing upstream pressure by 600 psia and using the same GOR values. The hypothesis here was that the two methods would, at the very least, behave in a similar fashion if no firm agreement could be made on exact liquid flow rates. Note the lower pressure trials at 2,400 psia and how the liquid rate drops as a consequence of increased GOR. However, the OLGA® simulation calculates a drop of about 11.5% in liquid flow rate whereas the Gilbert equation shows a decrease of 37.1% in liquid flow rate. Considering the higher 3,000 psia scenarios, the result is reversed; liquid rates increase with the GOR. At these larger pressures, the flow becomes critical and the Gilbert equation must be substituted for another designed to deal with such conditions. Equation 4.4, proposed by Wallis (1969), is used to verify if the multiphase flow is, in fact, critical.

$$V^* = \sqrt{\left(\rho_L \lambda_L + \rho_g \lambda_g\right)\left(\frac{\lambda_g}{\rho_g V_g^{*2}} + \frac{\lambda_L}{\rho_L V_L^{*2}}\right)} \tag{4.4}$$

The asterisk denotes critical flow for the overall fluid or the phase-specific flows. The in situ volume fractions, λ_g and λ_L, are generated with the OLGA® simulation just before the leak point. The critical fluid velocity differs for each phase however and must be computed with equations 4.5 and 4.6 below.

$$V_L^* = \frac{68.1}{\sqrt{\rho C}} \tag{4.5}$$

$$V_g^* = 41.4\sqrt{\frac{\kappa Z T}{\gamma_g}} \tag{4.6}$$

The parameters, such as the gas specific heat ratio (κ), the liquid compressibility factor (C), the gas compressibility (Z) and specific gravity of the gas (γ_g) are calculated with PVTsim®. Also, the temperature (T) is input with units of Rankine. Carrying out these operations indicates that the flow is indeed critical and provides the rates seen in Table 5.

Finally, Chapter 7 concludes with remarks about future work in this area, which may be improved with increased understanding of flow through various hole shapes. One tool of primary interest is CFD because it can visualize the streamline paths as fluid moves through a leak or restriction of abnormal geometry.

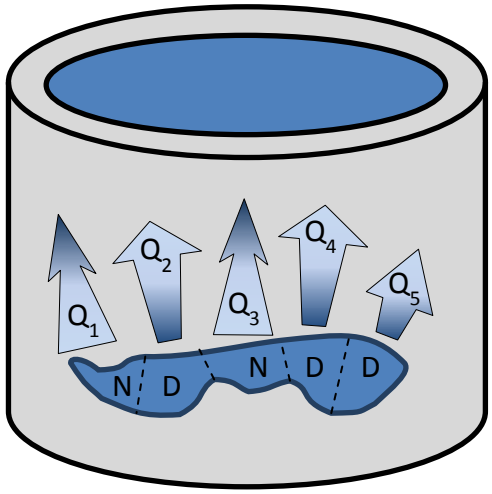

Figure 14. The arbitrary shape of a ruptured pipe may not exhibit simple flow paths, which complicates the computation of flow rate or pressure at that point. Converging and diverging streamlines can affect the fluid behavior at the effluent end of the system in unknown ways.

Chapter 5
Method and Procedure

A bank of modeled fluids was created, with details on compositions and saturation pressure types, from various sources (Ali and McCain, 2007 and El-Banbi, Fattah and Sayyouh, 2006). Additional modeled samples were developed from these in order to understand subtle nuances of compositional influence on a particular feature.

5.1 OLGA® Flow Model

Two vertical wells join together at the seafloor via 25-foot long tiebacks in the model per the problem statement in Chapter 2. Fluid flows from these tiebacks into a vertical length of pipe open to the sea. For simplicity, the profiles of the wells are identical, reaching down to 10,000 feet true vertical depth with a deviation starting at 8,000 feet. The deviation builds at approximately 3.5° per 100 feet. A schematic of the entire system as seen in OLGA® is displayed in Figure 15. The wells are constructed in two main parts, an upper portion and a lower one; the main differences between the two is the internal diameter of the production tubing increases from 4-½" in the lower part to 5-½" in the upper. To model the outlet to the sea floor a hydrostatic pressure of 2,200 psia is applied to the leak point. This is approximately the equivalent of 5,000 feet of sea water depth. The pressure will be greater than this as the leak will impart a pressure loss contingent upon its shape and the type fluids passing through it. Fluids exiting through this hole are assumed to be gas and oil only for modeling simplicity; the inclusion of water bears little significance, because most correlations for flow through an orifice do not distinguish different liquid phases. Additional complexity in the flow paths and the fluids can be handled by

the software, but also adds a layer of complexity to the analysis of the results that was deemed unnecessary.

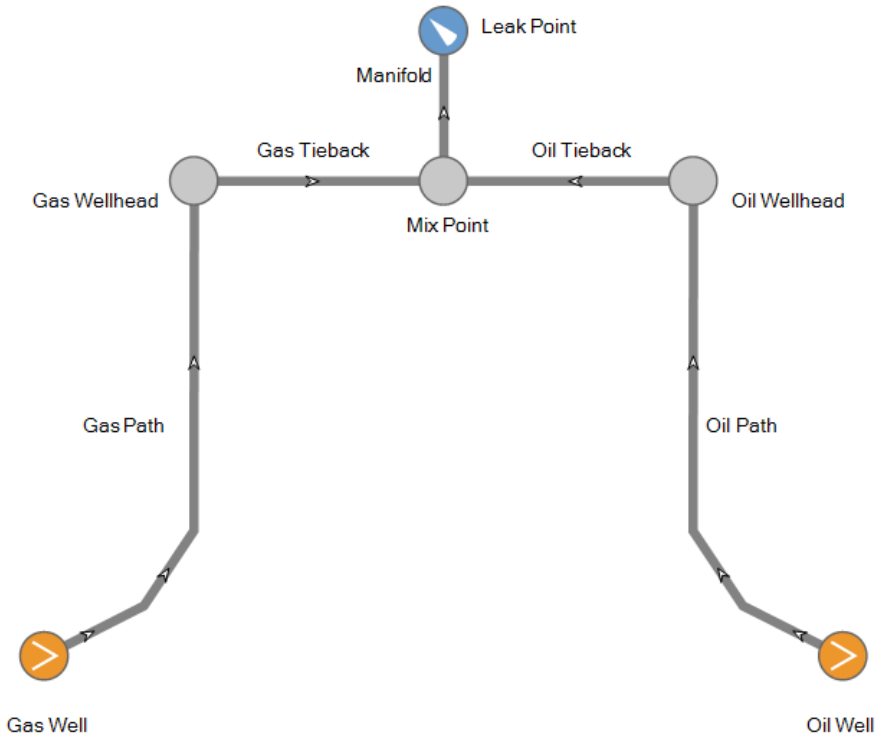

Figure 15. Two identical wells produce disparate fluids from unconnected reservoirs. All pertinent features of the wells and their associated boundary conditions, such as heat transfer coefficients, are equivalent to reduce extraneous parameters.

A great deal of consideration is given to the flow rates used under a variety of pressure conditions, but phase behavior also relies upon system temperature. This facet of the problem is underlined by the fact that hydrocarbons would escape to a relatively cold environment in deepwater environments. Therefore, heat-transfer coefficients are applied to the wells, pipelines and manifold. Heat moves through the system in different ways, so different definitions exist for the coefficients. Formation temperature increases with depth; that heat first penetrates the cement and the casing string it holds in place before traversing the annulus containing completion brines.

The dimensions of these items for both the upper section and the lower section of the well are seen in Figure 16.

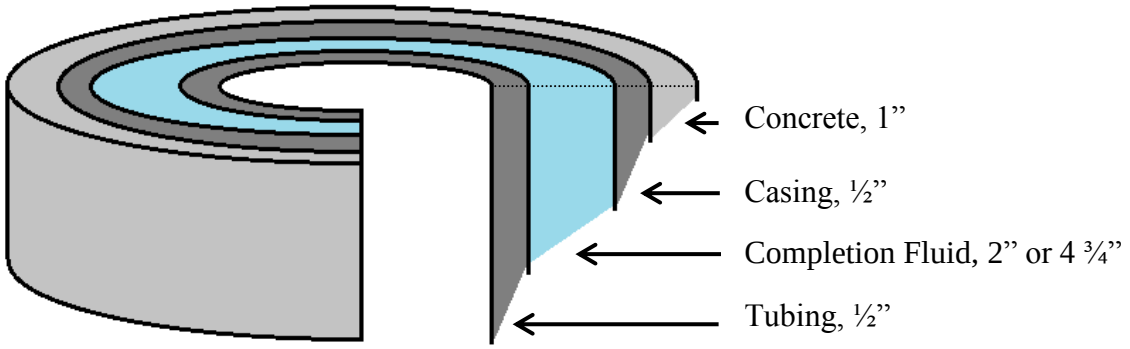

Figure 16. The physical properties of the tubing, casing, brine and cement are the same for both well sections except for the thickness of the annulus; a smaller liner is used at the bottom.

The barriers to heat transfer are in series and this leads to the form of Equation 4.3 for the overall heat-transfer coefficient, U_{to}, appearing similar to electric resistances in series.

$$\frac{1}{U_{to}} = \frac{r_{to}}{r_{ti}h_{to}} + \frac{r_{to}\ln\left(r_{to}/r_{ti}\right)}{k_t} + \frac{r_{to}}{r_{ci}(h_c + h_r)} + \frac{r_{to}\ln\left(r_{ci}/r_{to}\right)}{k_{CompFluid}} + \frac{r_{to}\ln\left(r_{co}/r_{ci}\right)}{k_c} + \frac{r_{to}\ln\left(r_{cem}/r_{co}\right)}{k_{cem}} \qquad (4.3)$$

Units are consistent for U_{to} to have units of Btu/(hr-ft^2-°F); r denotes radius measured from the center of the production tubing, the k variables refer to heat conductivity and the h variables to specific heat-transfer coefficients (the subscript r is for radiative heat transfer and c for convective heat transfer). The terms are arranged to describe the resistance from the center outward. Subscripts i and o stand for inner and outer, respectively; t is used for tubing; c for casing; and cem for cement. This coefficient relies on a temperature gradient, so it must be calculated along the entire well profile to couple properly with the changing formation temperature (the geothermal gradient). A thorough discussion of calculations and example values are provided in Appendix B.

5.2 Phase Behavior Studies

Using PVTsim®, trends can be developed by uniformly modifying mixing ratios between two representative fluids of condensate gas and black oil. Molar mixtures are simply sums of two fluids, which is to say that mole fractions of a given component are added to the mole fraction of the same component in another fluid and then the whole mixture is normalized to one mole of substance. Ratios are defined with the lighter fluid first, so a 9:1 mixture is nine times more concentrated in the lighter fluid than the heavier; here, a gas condensate is mixed with black oil. Therefore, a mixture of 9:1 is within ten percent of the original condensate's composition and a 100:1 mixture would be within one percent of the original lighter-fluid's composition. Mixtures studied were varied per the scheme found in Table 6. These weightings inevitably drag the critical points of the mixture towards the main contributing fluid's original critical point.

Table 6. Ratios used in Condensate-Oil Mixtures

Fluid	1	2	3	4	5	6	7	8	9	10	11
Ratio	100:1	50:1	9:1	8:2	7:3	6:4	1:1	4:6	3:7	2:8	1:9

Originally, only the ratios between 9:1 and 1:9 were considered, but investigating the differences of a few keys properties for larger ratios warranted the inclusion of the lower gravity mixtures here. Notice that the first two ratios are spread much more widely than all of the other mixture ratios in the table. The addition of the black oil, even at only 10%, has a marked effect on the properties of the combined fluids. The converse, however, is not true as seen in Table 7, which contains the critical properties and total density of the resulting fluids. Starting on the left side, the lightest mixture is created with 100 parts condensate and one part black oil. Two intermediate ratios, 50:1 and 20:1, follow before the 9:1 ratio.

The right side of the table displays the higher gravity mixtures, modified in the same proportions. The relative change between the 9:1 mix and the lighter fluids as well as the relative change between the 1:9 and the heavy mixtures are tabulated for the three parameters considered.

Table 7. Justification of Mixture Ratios Used in the PVT Study

	Mixture ratios (light fluid : heavy fluid)							
	100:1	**50:1**	**20:1**	**9:1**	**1:9**	**1:20**	**1:50**	**1:100**
Critical Presssure, psia	4873	5033	5270	5232	1651	1557	1510	1494
	-6.9%	-3.8%	0.7%	-	-	-5.7%	-8.6%	-9.5%
Critical Temperature, °F	135.91	167.21	245.51	361.25	815.53	822.98	826.69	827.92
	-62.4%	-53.7%	-32.0%	-	-	0.9%	1.4%	1.5%
Total Density at Reservoir Conditions, lbs/ft^3	22.97	23.40	24.59	26.59	41.28	41.75	41.99	42.07
	-13.6%	-12%	-7.5%	-	-	1.1%	1.7%	1.9%

Table 6 provides some of the answers to flow aggregation without running computationally intensive models. Small contributions from the black oil well likely bring about the onset of multiphase flow more readily than the opposite situation of a little gas joining a majority oil flow. Conceptually, this makes sense because gas can dissolve into a black oil and make little difference other than perhaps increasing B_o. Should a droplet of oil become entrained into a gas stream though, it is unlikely that the fluid will remain a single vapor phase.

Phase diagrams can help characterize the type of fluid in a reservoir. Those broad definitions used for fluid categories, in turn, suggest the flow behavior the fluid will exhibit in production tubing. The results section will cover the various mixture phase envelopes (including internal vapor/liquid mole fraction lines) and the way in which they change.

Chapter 6
Discussion and Results

The background work done in chapter two revealed sensitivities to the present study by using current knowledge and tools. The fact that the IPR of a model offshore reservoir plots nearly horizontal in most cases shows that it is not a limiting factor in the accidental release of hydrocarbons. More to the point, the steeper areas of curvature in a typical IPR are not realized on the same time scale of blowouts, which may last a few months or less. Chapter 3 dealt with the particulars of how a study of this type is usually performed and the years of data upon which the simulation's routines are based. The results of the processes carried out in Chapter 5 will now be displayed and their significance explained in light of recent disasters.

6.1 Commingling Fluids with Various Pressures

The reservoirs are stated to have the requisite productivity index to flow continuously without a significant drop in pressure within the time scale of a blowout, so there will always be a contribution to the leaking manifold from both reservoirs. Varying the pressure in either reservoir reveals obvious conclusions about variables like temperature, liquid holdup and GLR. The liquid flow rate originating from the black oil well changes an appreciable amount due the variability in the bottomhole pressure (BHP) used in this study, as seen in Figure 17. The condensate well's BHP is maintained at 7,000 psia while the black oil well's BHP starts at 1,000 psia less and increases to 5,000 greater than the condensate's BHP (in other words, the black oil well BHP ranges from 6,000 to 12,000 psia). The liquid rate at the leak contributed by the condensate well changes less than one percent; it also exhibits classic condensate behavior of first decreasing in liquid flow rate as the black oil reservoir pressure is brought up and then

begins to increase in the amount of liquid throughput as the black oil well's pressure exceeds the condensate's by about 3,000 psia.

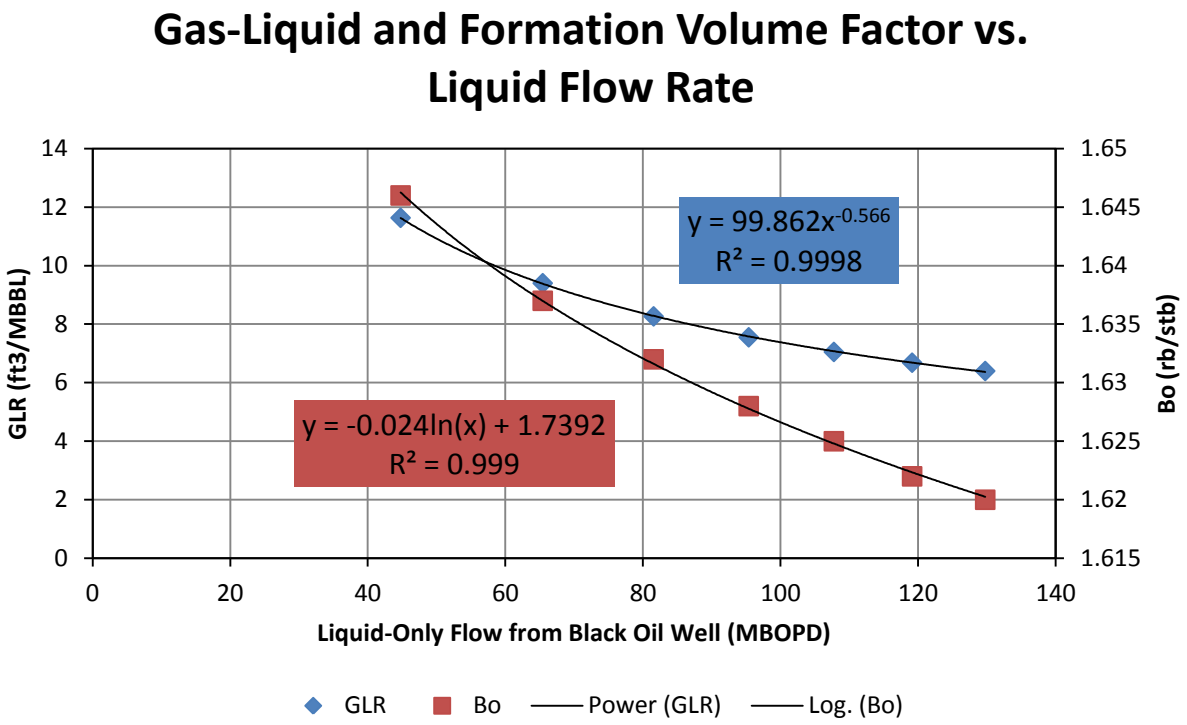

Figure 17. The GLR and B_o downstream of the mixing point can be estimated by using the flow rate contributed by the black oil well.

6.2 Influence of Mixture Ratio on Fluid Properties

The mixtures used in these case studies approach the composition of a constituent when a mixture ratio is biased enough toward that fluid, but there are interesting things to be noted in between these end-member cases. Quality lines do not change in the same fashion as saturation curves, leading to a propensity for liquid to fall out of a condensate or gas to evolve from a volatile oil while flowing up a well. The heavier hydrocarbons disproportionately affect the cricondentherm in these mixtures and interplays interestingly with lessons learned from OLGA® simulations seen in the next section concerning relative flow rates for various compositions.

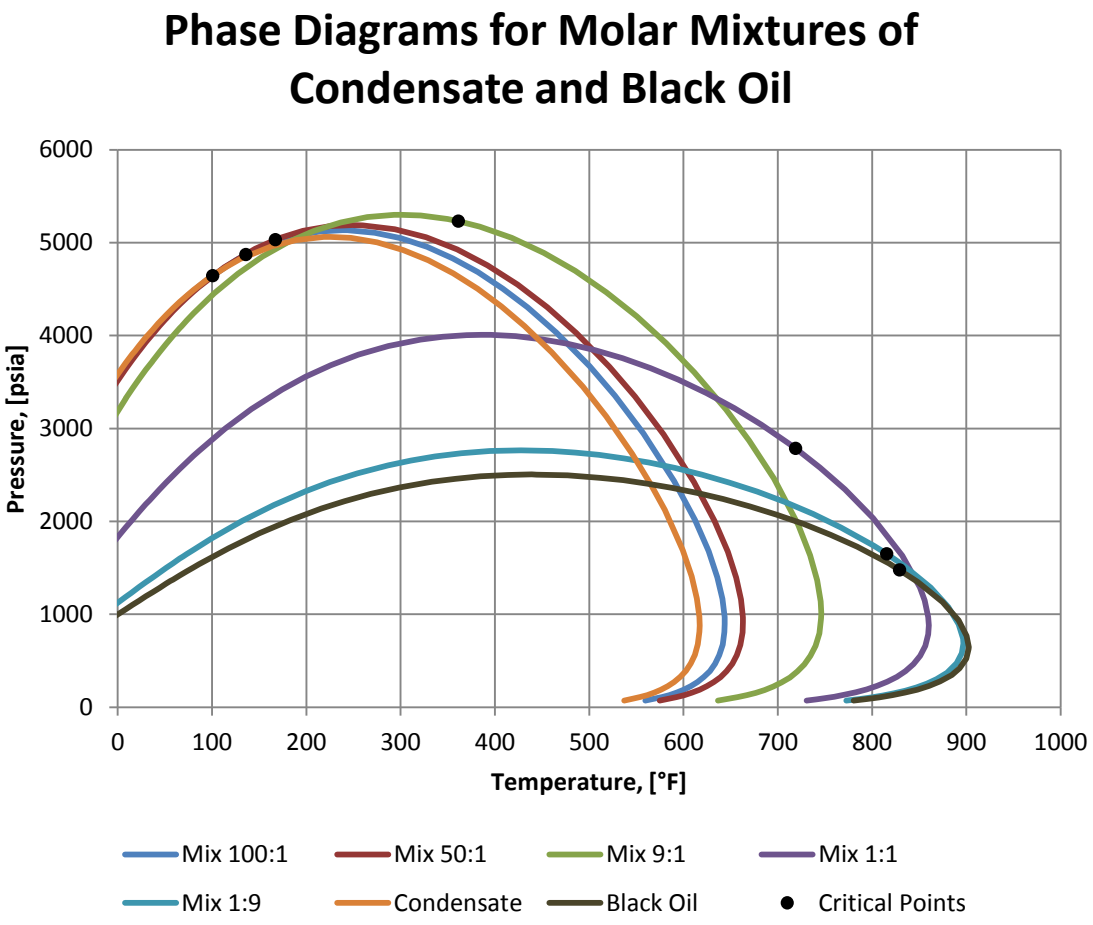

Figure 18. Phase envelopes shift to better reflect their largest constituent; this is most evident with the gradual change in height and width of the envelopes with successively heavier mixtures.

The cricondenbar and cricondentherm of a given mixture do not change much relative to the next mixture's maximum pressure and temperature as seen in Figure 18. However, the same cannot be said of the quality lines, which describe the percentages of phases contained within a system at equilibrium. For example, the cricondenbar doesn't change much when it drops 4.5% from Mix 9:1 to Mix 8:2 for the bubblepoint curve and about 5.4% for the 0.9 vapor/liquid mole fraction line. However, Figure 19 shows the cricondentherm increasing 6.5% on the dewpoint curve and 21.7% for the 0.9 vapor/liquid mole fraction line. This may carry consequences for a system that falls far below reservoir temperature, such as the case may be for pipes along the seafloor.

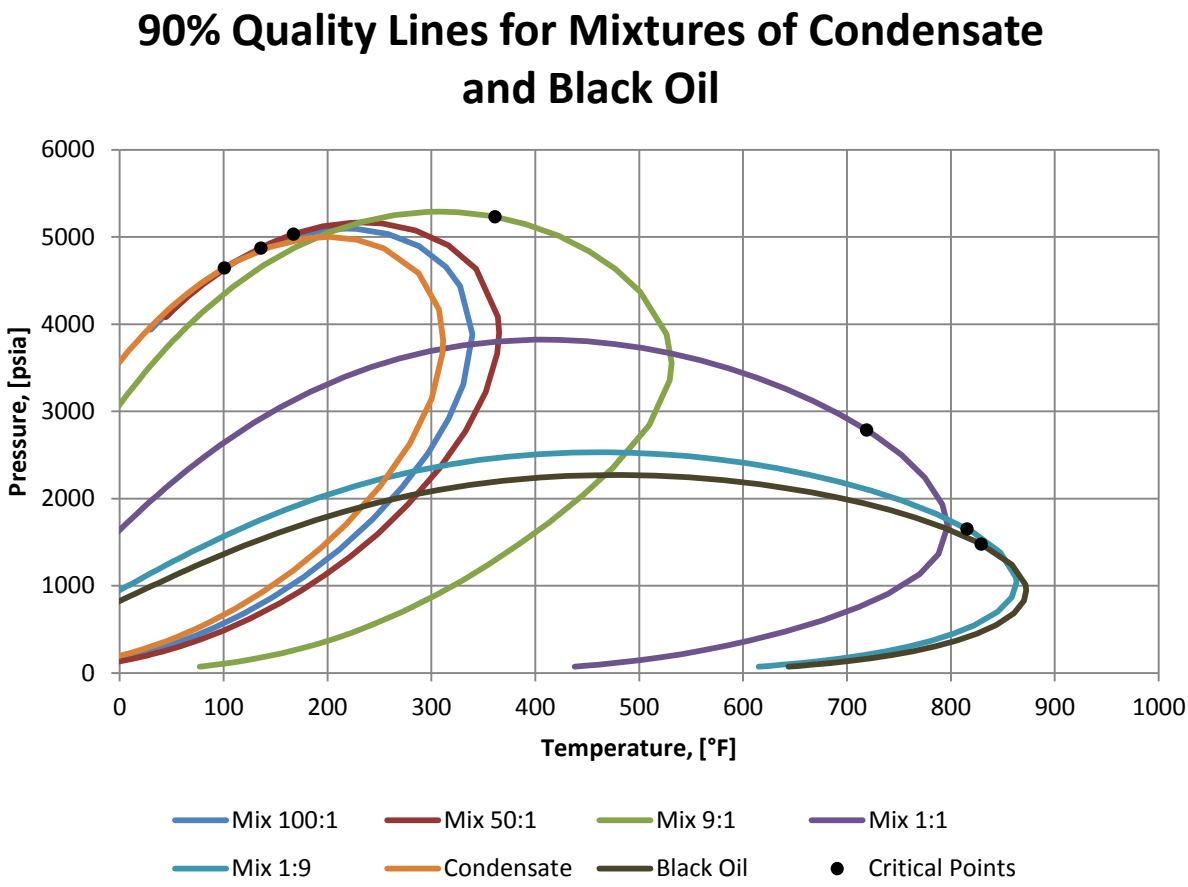

Figure 19. The same mixture ratios are maintained from Figure 9 and show the large departure of 0.9 vapor/liquid mole fraction lines from saturation curves.

Combining fluids per the phase behavior studies in Chapter 4 exposes the dependence of critical pressures and temperatures on C_{7+} fractions. Logically, these heavier components increase with the concentration of black oil in the mixture and are responsible for skewing the phase/quality envelopes to higher temperatures. The relevance here is the expansion or exsolution of gas near the leak point, further increasing volumetric flow rates. It is not until close inspection of composition that patterns begin to appear in ways that suggest a correlation that could be built for general mixing cases.

6.3 Compositional Effects in Simulation

The mixtures will seldom be neatly mixed like the ratios used in the previous PVTsim® study, so the original fluid streams are entered into OLGA® to combine more naturally. While this is intriguing in itself, varying the compositions of both fluids provides insight on how potentially damaging a leak can be.

6.3.1 Effect of Undersaturated Oil Coming in Contact with Condensate Gas

Table 8 lists, in thousands of barrels of liquid hydrocarbon per day, 25 combinations of different condensates and black oils flowing from the leak point.

Table 8. Liquid Flow Rates (BOPD) of Condensate-Black Oil Mixtures

	B-Oil 1	B-Oil 2	B-Oil 3	B-Oil 4	B-Oil 5
Cond 1	108.7	108.5	108.3	108.3	108.2
Cond 2	109.5	109.5	109.4	109.4	109.3
Cond 3	110.6	110.5	110.5	110.4	110.4
Cond 4	111.6	111.5	111.5	111.4	111.3
Cond 5	112.5	112.4	112.4	112.3	112.2

Note that the color change in the table indicates the lowest flow rate (108.2 BOPD at the top of the table) in red and the highest rate (112.5 BOPD at the bottom of the table) in green. An average formation volume factor of 1.814 (rb/stb) for the oil discharging to the sea should be used to convert these rates to surface rates. The gas rates for each fluid combination are listed in Table 9 with units of thousands of cubic feet per day. Again, these are not surface rates, so an average gas volume factor of 0.00457 should be used to convert these flow rates to surface

conditions. It is not advisable to simply divide by B_g here because the gas will partially dissolve in sea water, thereby reducing the quantity of gas actually seen at the surface. However, plume modeling from offshore spills is not within the scope of this study. For example, the solubility of methane in pure water at 2,250 psia is approximately $2x10^{-3}$ mole fraction (Rojey, 1997). One last point of interest is the general trend seen in the table, which contradicts intuition somewhat. The lightest black oil in combination with the heaviest condensate yields the most liquid and the heaviest black oil with the lightest condensate yields the least amount. Steady increments in liquid flow are to be expected from the gradual increase of the heptanes plus fraction in the condensate; however, the amount of liquid at the leak decreases slightly with each increase to the black oil's heavy fraction.

Table 9. Gas Leak Rates (Mcf/D) of Condensate-Black Oil Mixtures

	B-Oil 1	**B-Oil 2**	**B-Oil 3**	**B-Oil 4**	**B-Oil 5**
Cond 1	1,021.7	1,015.5	1,011.0	1,005.4	1,002.1
Cond 2	1,003.9	999.3	993.6	988.2	984.4
Cond 3	986.5	980.4	975.3	970.3	965.9
Cond 4	967.6	962.1	956.8	951.8	947.4
Cond 5	947.5	941.7	936.4	931.5	927.5

Now a table of GLR values can be generated and used for discharge computations. The question that remains though concerns the manner in which GLR changes from each wellhead to the mixing point. If a link can be established between these locations, then a correlation could be built to better predict leak rates if only bottomhole compositions are known.

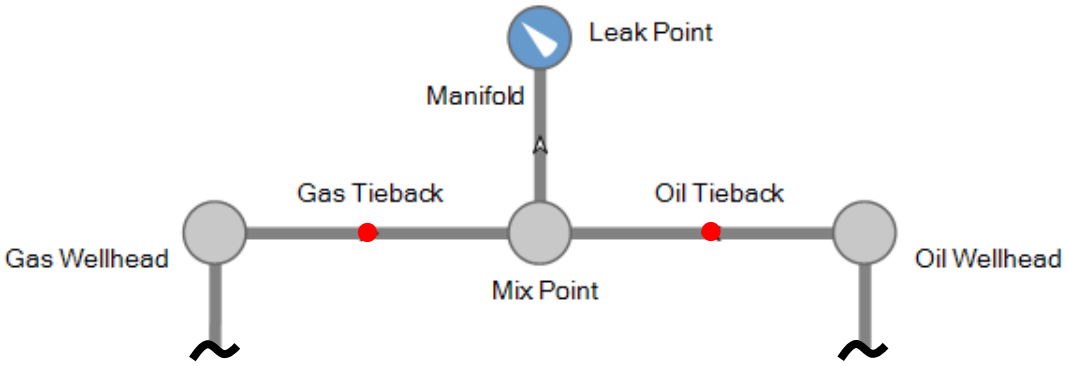

Figure 20. In order to assess the changes in GLR within the system, three sampling points are chosen. The first two places in which the compositions will be measured are the gas tieback and oil tieback, marked by red dots. The final sampling location is downstream of the T-joint at the leak itself.

Table 10. Gas-Liquid Ratios (ft^3/bbl) from the Gas Tieback Only

	B-Oil 1	**B-Oil 2**	**B-Oil 3**	**B-Oil 4**	**B-Oil 5**
Cond 1	10.460	10.527	10.597	10.652	10.721
Cond 2	10.185	10.263	10.322	10.376	10.445
Cond 3	9.925	9.981	10.050	10.097	10.157
Cond 4	9.659	9.727	9.782	9.833	9.889
Cond 5	9.399	9.456	9.509	9.567	9.619

As expected, the heavier the condensate contributing to the flow, the lower the combined GLR becomes at the leak. The mixtures containing heavier black oils have higher GLR's compared to those mixtures with the lighter black oil. This can be explained by considering how the modeled reservoir fluids were created. All components heavier than hexane were uniformly increased by 5%, 10%, 15% and 20% over the original composition. Even though this reduces the volatile components in the black oil and allows it to dissolve more gas, the increased density of the

mixture actually impedes liquid flow from the black oil well. Liquid flow from the black oil well reduces by 3.6% between B-Oil 1 and B-Oil 5, regardless of the condensate with which it mixes.

Table 11. Percent Change in Gas-Liquid Ratios from Wellheads to Leak Point.

	B-Oil 1	B-Oil 2	B-Oil 3	B-Oil 4	B-Oil 5
Cond 1	-11.26%	-12.53%	-13.57%	-14.71%	-15.79%
Cond 2	-11.14%	-12.48%	-13.68%	-14.83%	-15.98%
Cond 3	-11.29%	-12.54%	-13.84%	-14.90%	-16.05%
Cond 4	-11.39%	-12.76%	-13.96%	-15.09%	-16.20%
Cond 5	-11.59%	-12.89%	-14.12%	-15.31%	-16.40%

The black oil, with a bubble point of about 1,480 psia, is undersaturated up to the mixing point; therefore, the GLR in the oil tieback is equal to R_{soi} in all 25 permutations. Table 11 shows the amount the GLR changes from the wellheads to the leak. As the color coding indicates, the GLR does not correlate as strongly with the condensate well as it does with the black oil well.

6.3.2 Estimating GOR with Heptanes Plus Fraction

Using the same bank of 25 fluids, an effort was made to extrapolate fluid properties from only knowing the C_{7+} fraction of each fluid. McCain (1994) discusses the control heavy components have over reservoir fluid behavior and generalizes fluid characterization upon C_{7+} concentration and a few other parameters. Figure 21 is reproduced from McCain (1994) to show the dependence of initial GOR on heptanes-plus and how it may be used to make correlations.

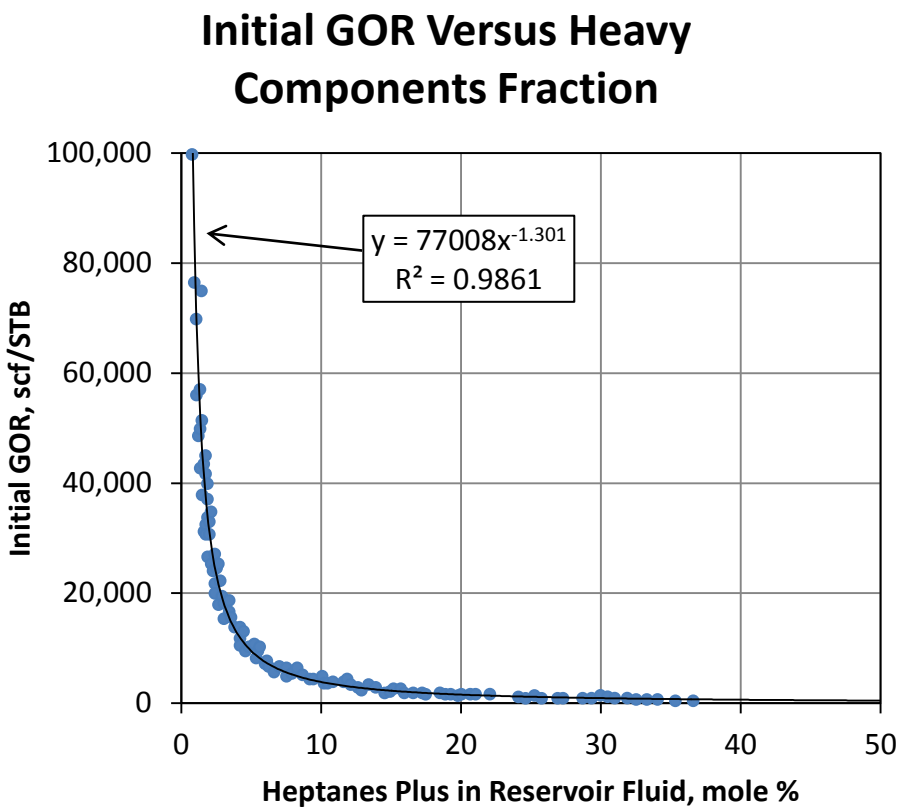

Figure 21. The initial gas-oil ratio ties together rather nicely with the amount of C_{7+} present in the reservoir fluids surveyed by McCain (1994). This chart includes fluids ranging from black oils to wet gases.

Although Figure 21 was reproduced from McCain's (1994) data set, the curve-fitting was calculated and may not match exactly as an explicit equation is not provided in the paper. Converting the GLR's from Table 10 allows the fluids studied herein to be plotted on this same chart. Despite lacking as many data points, a trend line for the data can still be constructed. Figure 22 appears promising, but the exponent determined for the trend line is too different for the correlation to McCain's data to be used for fluid mixtures involving anything lighter than condensate gases. The percent error below a heptanes-plus concentration of 10%, where the study takes place, should be considered the lower limit when using this relationship.

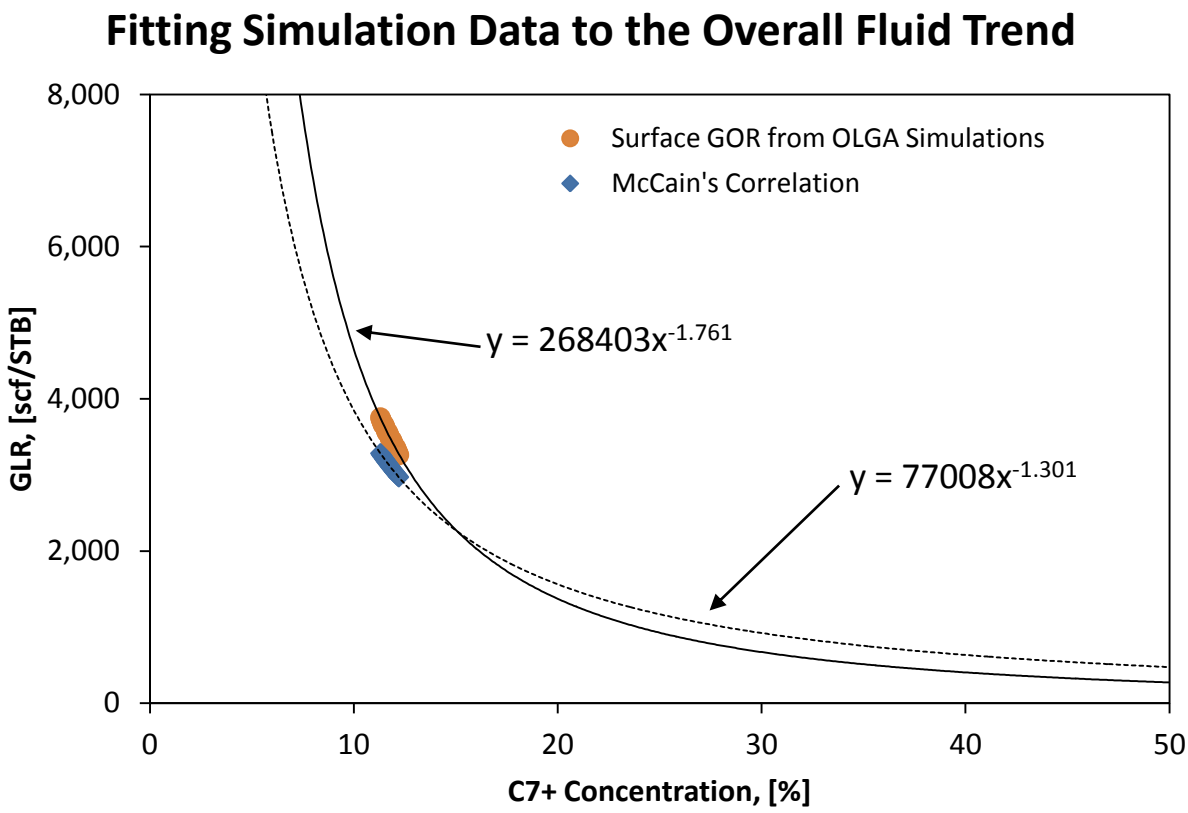

Figure 22. The 25 data points extracted from the OLGA® simulations are used to fit a power law trend line like the one used in McCain (1994).

If the range of fluids considered is reduced to those containing between approximately 5% and 20% heptanes-plus, then a clearer picture of how well this correlation works is visible. Figure 23 zooms further in on this section of the curve and compares the results of different methods available for predicting the gas-oil ratio from the heavies fraction. Since the trend line for the McCain data is grounded in several points of actual data, it is plotted again and used as a metric for determining how well the other methods might predict actual fluids. In addition, a ±10% error window for this data is also shown.

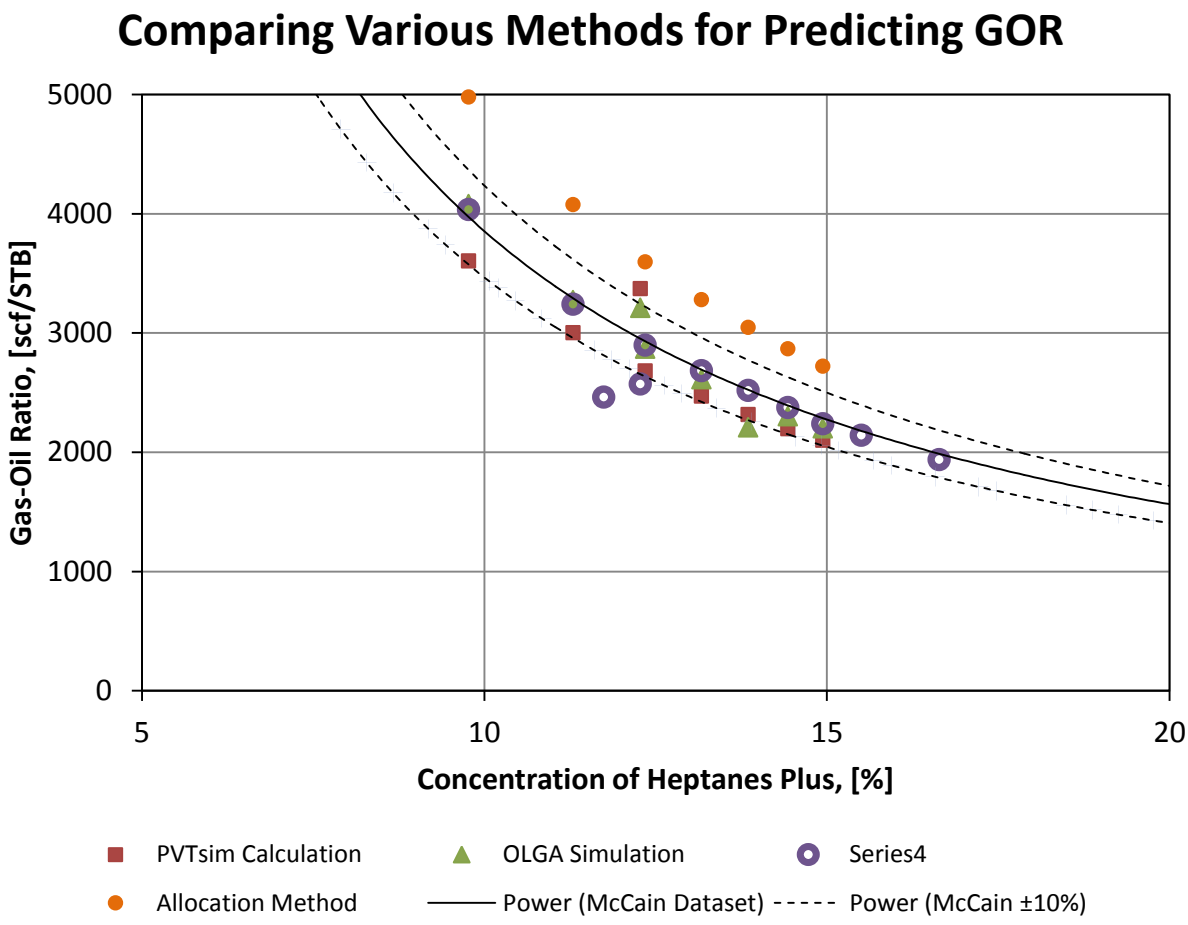

Figure 23. A suite of options exist for estimating the gas-oil ratio when limited data is available; most of these require the composition to be fully specified.

First, a number of trials were run in the OLGA® simulator with various pressures for each reservoir to furnish data points for curve-fitting. The gas condensate reservoir pressure was held constant at 7,000 psia initially while the black oil reservoir pressure was set to 6,000 psia and increased by 1,000 psia increments for each new trial. Compositions were sampled within the OLGA® simulation results at two points: just before mixing and at the leak point. The methods calculated by PVTsim® and OLGA® require the full composition to generate mixtures. However, only the heptanes-plus fractions found just before mixing are needed for calculating GORs with the proposed correlation. Regardless of method, once a mixture's heavies-fraction can be

determined, McCain's correlation can be applied to estimate the resulting fluid GOR. Assuming the physics modeled in OLGA® are correct, then the C_{7+} fraction listed at the leak point after simulation should provide input for McCain's correlation to get a close approximation of gas-liquid ratios expected at the seafloor (after adjusting for pressures and temperatures). Figure 23 does not show the GOR calculated with McCain's correlation with this heptanes-plus fraction as it would simply fall along the trend line shown. However, the GORs provided by the simulator are plotted as "OLGA® Simulation" in green triangles to compare with this line and fall within less than 4% save for one outlier that underestimates GOR by about 12%.

PVTsim® can do something different with the leak point compositions, though, by flashing them to surface conditions. These results are labeled "PVTsim® Calculation" and are marked by red squares in Figure 23 and agree with the McCain correlation to within less than ten percent. Another of PVTsim®'s tools is the allocation method previously described at the end of Chapter 3. This software routine consistently predicts GORs to be 20% to 25% higher than the McCain correlation. Implementing the allocation method is perhaps the quickest if flow rates and composition are known at the pressure and temperature of interest. However, one can estimate with even less information by using only the flow rates and heptanes-plus fraction. McCain's (1994) discussion of the influence of heavy components to reservoir fluid behavior partly led to the development of this faster calculation method.

The proposed correlation, denoted by purple circles in Figure 23, requires the volumetric flow rates, and their respective densities, from each fluid stream as well as the heptanes-plus fraction for each. Normalizing each stream's mass flow contribution by the sum of all mass flows aggregating at the mixing point provides a weighting mechanism (see Equation 6.1) for the C_{7+} fractions at the mix point.

$$\sum_{s=1,2}\left(\frac{\sum_{p=1,2} Q_p^s \rho_p^s}{\sum_{s=1,2}\sum_{p=1,2} Q_p^s \rho_p^s}\right) Z_{C_{7+}}^s = Z_{C_{7+}}^{Mixture} \tag{6.1}$$

The subscripts *s* and *p* represent well stream source and phase, respectively, while $Z_{C_{7+}}$ denotes the molar fraction of heptanes-plus. However, it is noted that this simple weighting function increases in error as the difference in flow from one source dominates the other. In order to account for this, the increasing difference between actual C_{7+} concentration and the predicted C_{7+} concentration is plotted against the difference in pressure between the contributing reservoirs. Applying this fix removes the gradual drift from accuracy, which tends to increase in a parabolic manner as displayed in Figure 24.

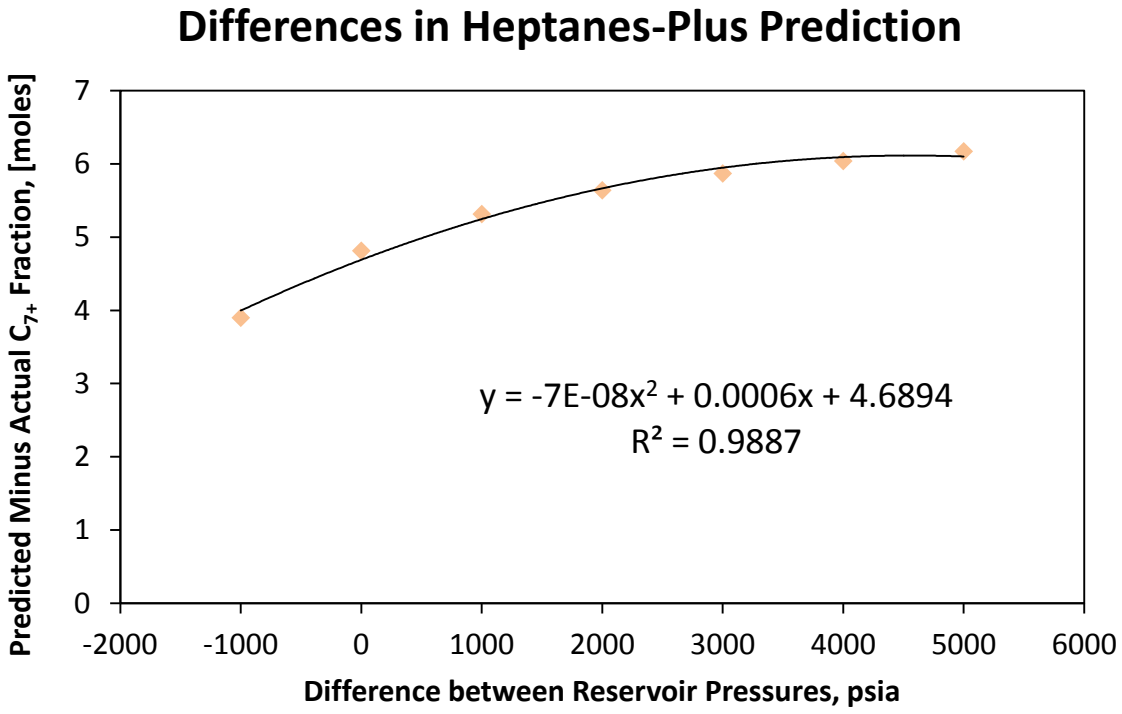

Figure 24. The increasing error in predicting the fraction of heavies within the combined fluids versus the relative strengths of the reservoirs is plotted. Here, the pressure of the condensate reservoir is subtracted from the black oil reservoir; the convention of subtracting the lighter-fluid reservoir pressure from the heavier-fluid reservoir must be maintained to use this correlation.

This correction need only be subtracted from the mixture's heptanes-plus fraction calculated in Equation 6.1 earlier.

$$Z_{C_{7+}}^{Mixture} + 7\times10^{-8}\Delta P^2 - 6\times10^{-4}\Delta P + 4.7 = Z_{C_{7+}}^{Mixture,Adjusted} \quad (6.1)$$

The ΔP here specifically refers to the pressure of the reservoir containing the denser fluid minus the reservoir pressure contributing the lighter fluid to the mixture. The procedure can be visualized in the flow diagram provided in Figure 25.

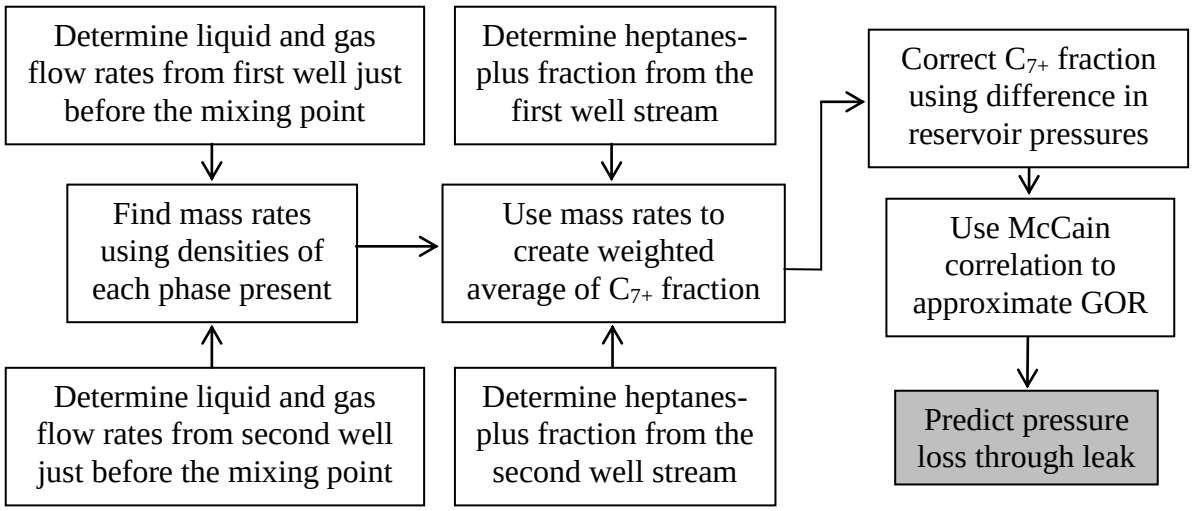

Figure 25. The process of combining disparate fluids from two different paths is procedurally short, but collection of pertinent data and actual calculation is better left to computer software.

Regarding the process in Figure 25 above, the starting point is always the same and focuses on simple knowledge of fluid properties and flow within the system. Simulators or nodal analysis can provide the relative rates of each contributing well or fluid source before the mixing point. Fluid samples can provide the heptanes-plus fraction of each stream, which will be weighted by the flow rates just determined. At this point, the method can vary some as the drift of predicted-to actual C_{7+} fraction will vary. Note that the abscissa in Figure 24 used to create the trend for

this drift is the heavier fluid's reservoir pressure minus the lighter fluid's reservoir pressure. This presents a problem for those situations containing more than one fluid source, but this may be handled with a hierarchical mixing scheme presented in Figure 26. Similar fluids are treated first with the proposed method to create pseudo-fluids, which are then combined with the disparate fluids (or pseudo-fluids) in turn.

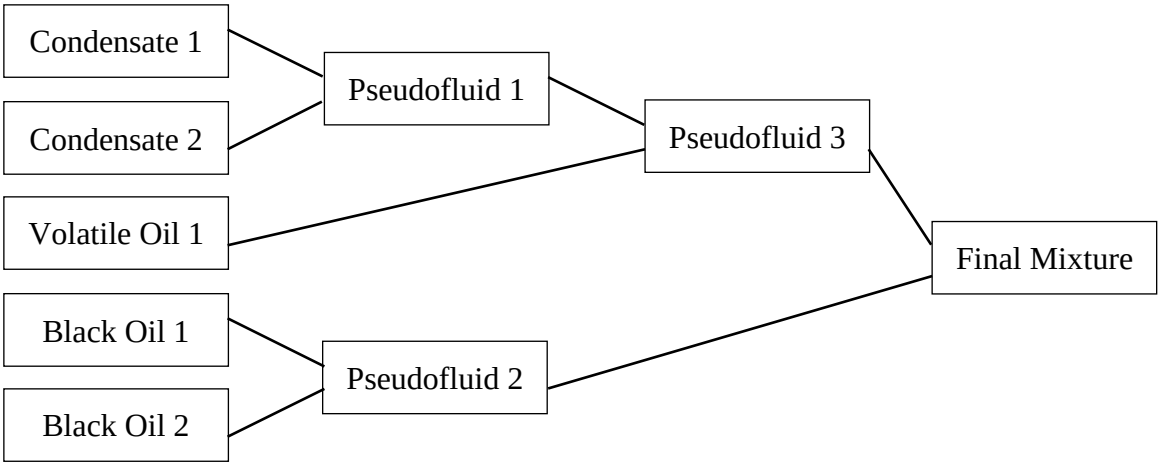

Figure 26. A hierarchy of mixing allows use of the proposed method with a complex mixture containing more than two constituent fluid sources.

The final prediction of C_{7+} mole fraction can then be used in the McCain relationship to find the mixture's GOR. This last piece of information is what the leak pressure drop hinges upon and provides greater accuracy in fluid discharge. One last thing to note is that the proposed correlation appears to predict a GOR lower than what is expected by the McCain correlation whereas the allocation method in PVTsim® consistently predicts too large a value (see Figure 23). The proposed correlation is preferred because it falls more closely within the spread of McCain's actual data points; however, an average between the new correlation and the allocation method may be used if either seems to err too much and both of these methods are very easy to obtain.

Chapter 7
Conclusions

The depths to which companies now drill require a tremendous amount of engineering, technology and capital. Producing from limited slots on platforms creates the need to operate satellite fields, which in turn opens up the risks associated with hydrocarbons releasing directly to the seafloor. Each aggregation in the network of flow lines is an area of mixing and possible leak point carrying fluids with seldom known properties. Knowing these fluid properties allows for relative rate calculations and the magnitude of the ensuing accident.

7.1 Performance Relationships Dependencies

Results of several simulations concerning aggregation of reservoir fluids, with varying physical and chemical properties, in a subsea field development have been presented. Chapter two began by setting up a generic scenario and discussed the most important parameters responsible for pressure losses. These variables were found within the tubing performance relationship primarily and, when changed even modest amounts, changed the flow rates much more than the properties of the reservoir. The one exception to this conclusion is the GOR of the fluid as the advent of multiphase flow greatly increases pressure drops in the flow path.

7.2 Position and Shape of Leak

Different locations of leak points and the hole geometries through which fluids escape were discussed. For the worst case of unobstructed flow from a pipe, data from Ashford (1974) was used to validate different methods of calculating choke flow. The initial attempt of modeling the leak with OLGA® did not produce accurate results, nor did it compare well with the alternatives discussed. A built-in correlation, utilizing a default value of 0.84 for the discharge coefficient,

allowed OLGA® to vastly improve the accuracy of its flow rate calculations. The coefficient can be changed to handle arbitrary leaks as one value will never suffice in a real-world situation. However, using Equation 4.1 provides an even better fit to the data furnished by Ashford (1974). In other words, finding a means to bring OLGA®'s built-in correlation to the level of Gilbert's will allow better estimations of hydrocarbon leaks. Determining a proper discharge coefficient continues to be the limiting factor regarding this improvement, but may be helped with the aid of CFD as discussed in the suggestions on future research below.

7.3 A New Correlation When Information is Scarce

The danger and irregularity associated with blowouts causes a good deal of difficulty when attempting to calculate discharge to the environment. Even when a reservoir has been mapped out and a well's profile is fully described, the manner in which merging fluids combine alters properties and behavior in uncertain ways. Either an expensive simulator or a TPR-IPR analysis can provide an idea of flow rates contributed by individual well streams. Complete fluid characterization or quantifying at least the heptanes-plus fraction in each constituent fluid allows for estimation of the heavies fraction. Ultimately, the GOR of the resulting mixture can be predicted with the correlation developed herein. This fluid parameter is important in the discharge equation originally put forth by Gilbert (1954) and improves understanding of pressure losses experienced at a leak point. This information can then be fed into the iterative solution process illustrated in Chapter 2.

7.4 Suggestions on Future Work

CFD modeling can greatly aid this study by fine-tuning the smaller elements of the system not captured by OLGA®. For instance, the wellhead flange connection need not be entirely rendered

in such a program (see Figure 27 for a small section of a typical flange and its mating gasket). Since the equipment is cylindrical, the symmetry can be exploited by only visualizing a quarter or eighth of the flange connection where a hole has eroded. A complete failure could be modeled in the same way, except without a gasket to abate flow, and the result multiplied by four or eight (depending on the modeler's preference of simplifying the geometry).

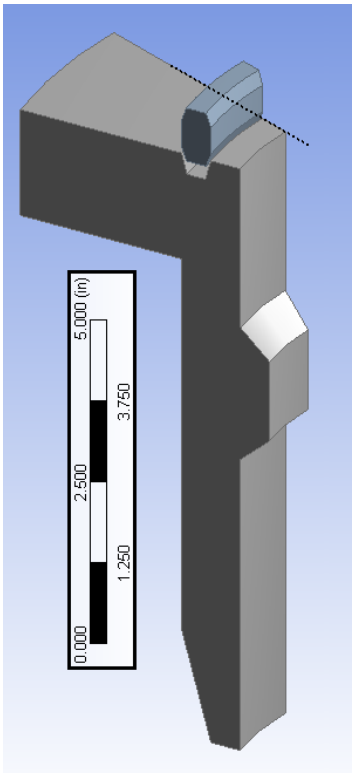

Figure 27. The modeling of a cylindrical well flange is simplified by considering only that portion which is leaking or by making a representative gap which circumscribe the connection.

Another consideration to make when expanding this study is the amount of wells contributing to the leak. Only two wells are considered presently, but the addition of a third well would complicate the mixing even further. However, the difference in fluid composition of the n^{th} well is not likely to be as different if it taps into the same reservoir as those nearby. If this assumption

is correct then the number of converging fluids can be reduced from the number of contributing wells to the number of disparate reservoirs contributing.

Bibliography

Ajienka, J.A., Enaibe, O.E. and Owolabi, O.O. 1994. Multiphase Flow Metering: An Evaluation of Discharge Coefficients. *Journal of Canadian Petroleum Technology* **33** (8): 57-62.

Al-Meshari, Ali A. and McCain, William. 2007. Validation of Splitting the Hydrocarbon Plus Fraction: First Step in Tuning Equation of State. Paper SPE 104631 presented at the 15th SPE Middle East Oil & Gas Show and Conference, Kingdom of Bahrain. March 11-14.

Anderson, D. 2012. *Flow Assurance with OLGA® 7.* SPT Group Industry Course. May 9-11.

Ansari, A.M., Sylvester, N.D., Sarica, C., Shoham, O., and Brill, J.P. 1994. A Comprehensive Mechanistic Model for Upward Two-Phase Flow in Wellbores. *SPE Production and Facilities* **9** (2): 143-151.

Ashford, F.E. 1974. An Evaluation of Critical Multiphase Flow Performance through Wellhead Chokes. *Journal of Petroleum Technology* **26** (8): 843-850.

Baxendell, P.B. and Thomas, R. 1961. The Calculation of Pressure Gradients in High-Rate Flowing Wells. Paper presented at Joint AIChE-SPE Symposium, Tulsa, Oklahoma. September 25-28, 1960.

Bendiksen, K.H., Malnes, D., Moe, R. and Nuland, S. 1991. The Dynamic Two-Fluid Model OLGA®: Theory and Application. *SPE Production Engineering* **6** (2): 171-180.

Bird, R.B., Stewart, W.E., and Lightfoot, E.N. 2007. *Transport Phenomena, 2nd edition*. Pages 12-84.

Brown, K.E. and Lee, J.F. 1985. Nodal Systems Analysis of Oil and Gas Wells. *Journal of Petroleum Technology* **37** (10): 1751-1763.

Courant, R., Friedrichs, K. and Lewy, H. 1967. On the Partial Difference Equations of Mathematical Physics. *IBM Journal of Research and Development* **11** (2): 215-234.

Craft, B.C., Hawkins, M.F., Jr. and Terry, R.E.: Applied Petroleum Reservoir Engineering. New Jersey: Hall, Inc.

Duns, H. and Ros, N.C.J. 1963. Vertical Flow of Gas and Liquid Mixtures in Wells. Paper presented at the 6th Annual World Petroleum Congress, Frankfurt am Main, Germany, June 19-26.

El-Banbi, A.H., Fattah, K.A. and Sayyouh, M.H. 2006. New Modified Black-Oil Correlations for Gas Condensate and Volatile Oil Fluids. Paper SPE 102240 presented at the SPE Annual Technical Conference and Exhibition, San Antonio, Texas, USA. September 24-27.

Engineering Toolbox. 2013. *Emissivity Coefficients of Some Common Materials*. Downloaded February 19.

Forrest, J., Marcucci, E. and Scott, P. 2005. Geothermal Gradients and Subsurface Temperatures in the Northern Gulf of Mexico. Search and Discovery Article #30048 in GCAGS Transactions 55: 233-248.

Gilbert, W.E. 1954. Flowing and Gas-Lift Well Performance. *Drilling and Production Practice* (API) 126-43.

Gulf of Mexico. 2013. Scale not determined; James Stiernberg; using "Google Maps". https://maps.google.com/maps?q=gulf+of+mexico&ll=27.771051,-90.615234&spn=7.345348,9.876709&hnear=Gulf+of+Mexico&t=h&z=7 (accessed March 11, 2013).

Hagedorn, A.R. and Brown, K.E. 1963. The Effect of Liquid Viscosity in Two-Phase Vertical Flow. Paper SPE 733 presented at the SPE Fall Meeting in New Orleans, 6-9 October.

Hasan, A.R. and Kabir, C.S. 2002. Fluid Flow and Heat Transfer in Wellbores. Richardson, TX: Society of Petroleum Engineers, Inc., pages 1-62.

Hein, M.A. 1987. Nodal Analysis as Applied to Pipelines and Risers. Paper presented at Pipeline Simulation Interest Group in Tulsa, Oklahoma, 22-23 October.

Iwere, F.O., Heim, R.N., and Cherian, B.V. 2012. Numerical Simulation of Enhanced Oil Recovery in the Middle Bakken and Upper Three Forks Tight Oil Reservoirs of the Williston Basin. Paper SPE 154937 presented at the Americas Unconventional Resources Conference in Pittsburgh, PA, June 5-7.

Job, G. and Herrmann, F. 2006. Chemical Potential—A Quantity in Search of Recognition. *European Journal of Physics* **27** (2): 353-371.

Langlinais, J. 2013. Two Phase Flow. File last modified March 2013. *Microsoft Excel* file.

Lietz, W. Tempelaar. 1949. The Performance of the Ten Section Oil Field. *Journal of Petroleum Technology* **1** (9): 251-258.

Mach, J., Proano, E., and Brown, K.E. 1979. A Nodal Approach for Applying Systems Analysis to the Flowing and Artificial Lift Oil or Gas Well. OnePetro, http://www.onepetro.org/. Accessed 26 February 2012.

Massoud, M. 2005. Engineering Thermofluids: Thermodynamics, Fluid Mechanics and Heat Transfer. Berlin: Springer.

McCain, William D. 1990. The Properties of Petroleum Fluids, Second Edition. Tulsa, Oklahoma: PennWell Books.

McCain, William D. 1994. Heavy Components Control Reservoir Fluid Behavior. *Journal of Petroleum Technology* **46** (9): 746-750.

Millheim, K., Williams, T.E., Yemington, C.R. 2011. Evaluation of Well Testing Systems for Three Deepwater Gulf of Mexico (GOM) Reservoir Types. Paper SPE 145682 prepared for the SPE Annual Technical Conference and Exhibition in Denver, CO, Oct. 30-Nov. 2

Moore, T.V. and Wilde, H.D. 1931. Experimental Measurements of Slippage in Flow through Vertical Pipe. *Trans. Am. Inst. Mining Met. Engrs. (Petroleum Development and Technology)* **114** (99): 296-319.

Muskat, M. 1949. Physical Principles of Oil Production. New York: McGraw-Hill.

Navier, L.M.H. 1827. Mémoires de l'Académie Royale des Sciences **6**: 389-440.

Nichol, J.R. and Kariyawasam, S.N. 2000. Risk Assessment of Temporarily Abandoned or Shut-in Wells. Report for the Department of Interior, Mineral Management Service.

Nodine, M.C., Wright, S.G., Gilbert, R.B. and Ward, E.G. 2006. Mudflows and Mudslides During Hurricane Ivan. Paper presented at the Offshore Technology Conference in Houston, Texas, May 1-4.

OLGA®. 2012. Computer software manual by SPT Group. Version 7.2, released September 27.

Payne, L. and Sandeen, J. 2013. Emerging Plays Boost Economic Attractiveness of Deepwater Gulf of Mexico. *The Way Ahead* **9** (1): 11-13.

Pedersen, K.S. and Milter, J. 2004. Phase Equilibrium Between Gas Condensate and Brine at HT/HP Conditions. Paper SPE 90309 presented at the SPE Annual Technical Conference and Exhibition in Houston, Texas, September 26-29.

Pedersen, K.S. 2005. PVT Software Applied with Multiphase Meters for Oil & Gas Allocation. Presented at the Flow 2005: Modeling, Metering and Allocation conference in Aberdeen, Scotland, March 14-15.

Peneloux, A., Rauzy, E., Freze, R. 1982. A Consistent Correction for Redlich-Kwong-Soave Volumes. *Phase Equilibria* **8** (1): 7-23.

Peng, D. and Robinson, D.B. 1976. A New Two-Constant Equation of State. *Ind. Eng. Chem. Fundamentals* **15** (1): 59-64.

Poettmann, F.H. and Carpenter, P.G. 1952. The Multiphase Flow of Gas, Oil, and Water Through Vertical Flow Strings with Application to the Design of Gas-Lift Installations. Presented at the spring meeting of the Mid-Continent District, Division of Production, Wichita, Kansas, March.

PVTsim®. 2012. Computer software manual by Calsep. Version 20.2.0, released April 9.

Rahman, M.M., Biswas, R. and Mahfuz, W.I. 2009. Effects of Beta Ratio and Reynold's Number on Coefficient of Discharge of Orifice Meter. *Journal of Agricultural and Rural Development* **7** (1&2): 151-156.

Redlich, O. and Kwong, J.N.S. 1949. On the Thermodynamics of Solutions. V—An Equation of State. Fugacities of Gaseous Solutions. *Chem. Reviews* **44**: 233-244.

Riazi, M. R. and Mansoori, G.A. 1992. An Accurate Equation of State for Hydrocarbon Systems. Paper SPE 25397 available from SPE, Richardson, Texas.

Rojey, A. 1997. Natural Gas: Production, Processing, Transport. Paris, France: Technip, pages 205-207.

Ros, N.C.J. 1961. An Analysis of Critical Simultaneous Gas/Liquid Flow through a Restriction and Its Application to Flow Metering. *Applied Science Research* **9**: 843-850.

Soave, G. 1972. Equilibrium Constants from a Modified Redlich-Kwong Equation of State. *Chem. Eng. Sci.*, **27** (6): 1197-1203.

Stokes, G.G. 1845. Proceedings of the Cambridge Philosophical Society **8**: 287-319.

Tannehill, J.C., Anderson, D.A. and Pletcher, R.H. 1997. Computational Fluid Mechanics and Heat Transfer Second Edition. Washington, D.C.: Taylor & Francis, pages 45-60.

Trefethen, L.N. 1996. Finite Difference and Spectral Methods for Ordinary and Partial Differential Equations. Unpublished text available at http://people.maths.ox.ac.uk/trefethen/pdetext.html. Downloaded 29 October 2012.

van der Waals, J.D. 1873. Over de Continuiteit van den Gas-en Vloeistoftoestand. Dissertation, Leiden University, Leiden, Netherlands.

Walsh, M.P. and Lake, L.W. 2003. A Generalized Approach to Primary Hydrocarbon Recovery. Oxford, UK: Elsevier, pages 209-210.

Weisstein, Eric W. "Courant-Friedrichs-Lewy Condition." From MathWorld--A Wolfram Web Resource. http://mathworld.wolfram.com/Courant-Friedrichs-LewyCondition.html

White, Frank M. 2006. Viscous Fluid Flow (3rd Edition). New York: McGraw-Hill.

Appendix

A. Fluid Bank

Fluids in this study came from different sources; Al-Meshari and McCain (2007) provide the initial condensate and black oil fluids denoted by the superscript-daggers in the following tables.

Table 12. Condensate Fluids Used in Studies and Some of Their Properties

Component or Property	Cond 1†	Cond 2	Cond 3	Cond 4	Cond 5
N_2	0.29	0.2891	0.2882	0.2872	0.2863
CO_2	0.2	0.1994	0.1987	0.1981	0.1975
C_1	84.66	84.3900	84.1216	83.8550	83.5900
C_2	4.04	4.0271	4.0143	4.0016	3.9889
C_3	2.23	2.2229	2.2158	2.2088	2.2018
C_4	0.68	0.6778	0.6757	0.6735	0.6714
C_5	0.99	0.9868	0.9837	0.9806	0.9775
C_6	0.51	0.5084	0.5068	0.5052	0.5036
C_7	1.12	1.1722	1.2242	1.2758	1.3270
C_8	0.51	0.5338	0.5574	0.5809	0.6043
C_9	0.38	0.3977	0.4153	0.4328	0.4502
C_{10}	0.3	0.3140	0.3279	0.3417	0.3555
C_{11}	0.28	0.2931	0.3060	0.3189	0.3318
C_{12}	0.22	0.2303	0.2405	0.2506	0.2607
C_{13}	0.2	0.2093	0.2186	0.2278	0.2370
C_{14}	0.15	0.1570	0.1640	0.1709	0.1777
C_{15}	0.12	0.1256	0.1312	0.1367	0.1422
C_{16}	0.12	0.1256	0.1312	0.1367	0.1422
C_{17}	0.1	0.1047	0.1093	0.1139	0.1185
C_{18}	0.07	0.0733	0.0765	0.0797	0.0829
C_{19}	0.06	0.0628	0.0656	0.0683	0.0711
C_{20}	0.05	0.0523	0.0547	0.0570	0.0592
C_{21}	0.04	0.0419	0.0437	0.0456	0.0474
C_{22}	0.03	0.0314	0.0328	0.0342	0.0355
C_{23}	0.03	0.0314	0.0328	0.0342	0.0355
C_{24}	1.5	1.5700	1.6395	1.7086	1.7773
C_{25}	0.95	0.9943	1.0384	1.0821	1.1256
Pseudocomponent C_{26}-C_{30}	0.09	0.0942	0.0984	0.1025	0.1066
Pseudocomponent C_{31}-C_{36}	0.08	0.0837	0.0874	0.0911	0.0948
Critical Pressure (psia)	4645.2	4748.3	4826.8	4890.4	4941.2
Critical Temperature (°F)	100.7	117.5	132.1	146.1	159.5

The compositional tracking module in OLGA® requires an input called a "feedfile" which limits the amount of components used to thirty, thereby increasing the granularity of simulation results; this is mitigated by choosing components similar to each other in any given pseudocomponent. For example, one pseudocomponent definition groups normal and iso-butane. Thus, the maximum is used with no pseudocomponent representing more than six individual components).

Table 13. Black Oils Used in Studies and Some of Their Properties

Component or Property	**B-Oil 1**†	**B-Oil 2**	**B-Oil 3**	**B-Oil 4**	**B-Oil 5**
N_2	0.7960	0.7828	0.7700	0.7576	0.7456
CO_2	1.1940	1.1742	1.1550	1.1364	1.1184
H_2S	0.4980	0.4897	0.4817	0.4740	0.4665
C_1	44.0300	43.2987	42.5913	41.9067	41.2437
C_2	5.4730	5.3821	5.2942	5.2091	5.1267
C_3	5.2740	5.1864	5.1017	5.0197	4.9402
C_4	2.0900	2.0553	2.0217	1.9892	1.9577
C_5	3.383	3.3268	3.2725	3.2199	3.1689
C_6	3.4830	3.4252	3.3692	3.3150	3.2626
C_7	2.8860	2.9800	3.0709	3.1588	3.2440
C_8	2.1890	2.2603	2.3292	2.3960	2.4606
C_9	1.9200	1.9825	2.0430	2.1015	2.1582
C_{10}	1.6920	1.7471	1.8004	1.8520	1.9019
C_{11}	1.6120	1.6645	1.7153	1.7644	1.8120
C_{12}	1.4330	1.4797	1.5248	1.5685	1.6108
C_{13}	1.3330	1.3764	1.4184	1.4590	1.4984
C_{14}	1.1440	1.1812	1.2173	1.2522	1.2859
C_{15}	0.9550	0.9861	1.0162	1.0453	1.0735
C_{16}	0.9550	0.9861	1.0162	1.0453	1.0735
C_{17}	0.9050	0.9345	0.9630	0.9906	1.0173
C_{18}	0.7160	0.7393	0.7619	0.7837	0.8048
C_{19}	0.6470	0.6681	0.6884	0.7082	0.7273
C_{20}	0.5970	0.6164	0.6352	0.6534	0.6711
C_{21}	0.5470	0.5648	0.5820	0.5987	0.6149
C_{22}	0.5070	0.5235	0.5395	0.5549	0.5699
C_{23}	0.4780	0.4936	0.5086	0.5232	0.5373
C_{24}	3.3830	3.4932	3.5997	3.7028	3.8027
C_{25}	2.587	2.6712	2.7527	2.8316	2.9079
Pseudocomponent C_{26}-C_{30}	1.91	1.9722	2.0323	2.0906	2.1470
Pseudocomponent C_{31}-C_{36}	5.383	5.5583	5.7278	5.8919	6.0508
Critical Pressure (psia)	1480.8	1434.9	1392.4	1353	1316.4
Critical Temperature (°F)	829.8	834.7	839.2	843.3	847.2

B. Heat-Transfer Coefficient Calculations

The overall heat-transfer coefficient equation is reproduced here from Chapter 4's section discussing the OGLA model.

$$\frac{1}{U_{to}} = \frac{r_{to}}{r_{ti}h_{ti}} + \frac{r_{to}\ln\left(r_{to}/r_{ti}\right)}{k_t} + \frac{r_{to}}{r_{ci}(h_c + h_r)} + \frac{r_{to}\ln\left(r_{ci}/r_{to}\right)}{k_{ann}} + \frac{r_{to}\ln\left(r_{co}/r_{ci}\right)}{k_c} + \frac{r_{to}\ln\left(r_{cem}/r_{co}\right)}{k_{cem}} \tag{B.1}$$

The greatest difficulty in determining this number is the temperature-dependent nature of the heat-transfer coefficients associated with convection. A number of heat-transfer coefficients must first be found before incorporating all of them together; for example, the first term deals with conductive heat transfer from the reservoir fluid to the outside surface of the production tubing.

$$h_{ti} = 0.023\frac{k_{HC}}{d_{ti}}\mathrm{Re}^{0.8}\,\mathrm{Pr}^{1/3} = 0.023\frac{k_{HC}}{d_{ti}}\left(\frac{\rho v d}{\mu_{HC}}\right)^{0.8}\left(\frac{c_p\mu_{HC}}{k_{HC}}\right)^{1/3}\left(\frac{\mu_{HC}}{\mu_w}\right)^{0.14} \tag{B.2}$$

The produced fluid's thermal conductivity, k_{HC}, and viscosity, μ_{HC}, are required for the Reynolds number (*Re*) and the Prandtl number (*Pr*); these dimensionless numbers are expanded in Equation B.2 for convenience. The former is a ratio of viscous and inertial forces while the latter, Prandtl number, is a ratio of momentum diffusivity to thermal diffusivity (White, 2006). An initial OLGA® simulation is required to obtain an idea of what the superficial fluid velocity is at the bottom of the well; it is about 36.4 ft/s in the black oil well. The other items required for these equations, such as dimensions and emissivity, are given in Table 8.

Table 14. Well Profile and Material Properties Used in Thermal Calculations

Parameter		**Lower Portion**	**Upper Portion**
d_{ti} (in)	=	4.5	5.5
d_{to} (in)	=	5	6
d_{ci} (in)	=	7	10.75
d_{co} (in)	=	7.5	11.25
d_{cem} (in)	=	8.5	12.25
$\varepsilon_{steel,\ polished}$†	=	0.075	0.075
k_{oil} (Btu/hr-ft-°F)	=	0.131	0.132
$c_{p,oil}$ (Btu/lbmol-°F)	=	56.63	52.95
ρ_{oil} (lbs/ft^3)	=	53.04	53.04
ρ_{ann} (lbs/ft^3)	=	59.14	63.1
μ_{oil} (lb/ft-hr)	=	1.78	1.773
μ_{ann} (lb/ft-hr)	=	0.8696	3.67
k_{ann} (Btu/hr-ft-°F)	=	0.406	0.37
$k_{tbg,csg}$ (Btu/hr-ft-°F)	=	11.54	11.54
k_{cem} (Btu/hr-ft-°F)	=	4.021	4.021
β_{oil} (1/°F)	=	0.314	0.314
MW_{oil} (lb/lbmol)	=	101.22	101.22

† Measured at 300 Kelvin according to The Engineering Toolbox (2013).

Plugging the proper terms in yields the Reynolds number, the Prandtl number and the first conductivity value (which has units of Btu/hr-ft^2-°F).

$$\mathrm{Re} = \frac{\rho_{oil} v d}{\mu_{oil}} = \frac{53.04 * 36.4 * 0.375}{(1.78/3600)} = 1{,}464{,}168 \tag{B.3}$$

$$\mathrm{Pr} = \frac{c_{p,oil}\mu_{oil}}{k_{oil} MW_{oil}} = \frac{56.63 * 1.78}{0.131} * \frac{1}{101.22} = 7.6 \tag{B.4}$$

$$h_{ti} = 0.023 \frac{0.131}{0.375} \left(1{,}464{,}168^{0.8}\right)\left(7.6^{1/3}\right)\left(\frac{1.78}{0.8696}\right)^{0.14} = 1{,}494.85 \tag{B.5}$$

The next heat-transfer coefficients that require some involved manipulation relate to radiation and convection in the annular space between tubing and casing. The Grashof number (*Gr*) must be introduced to proceed with the calculation of the convection term.

$$Gr = (r_{ci} - r_{to})^3 g\rho_a^2 \beta \left| \frac{T_{ci} - T_{to}}{\mu_a^2} \right| = \left(\frac{3.5}{12} - \frac{2.5}{12} \right)^3 (32.2 * 59.14^2 * 0.314) \left| \frac{179 - 180}{0.8696^2} \right| = 30.16 \qquad \text{(B.6)}$$

The gravity constant, *g*, uses length units consistent with the density and the fluid expansion term, β, has units of reciprocal Fahrenheit. Convective heat transfer within the completion brine between tubing and casing can now be determined.

$$h_c = \frac{0.049(Gr\,\mathrm{Pr})^{1/3}\,\mathrm{Pr}^{0.074} k_{ann}}{r_{ci} \ln\left(r_{ci} / r_{to} \right)} = \frac{0.049 * (30.16 * 7.6)^{1/3} (7.6^{0.074}) 0.347}{\left(\frac{7}{2 * 12} \right) \ln\left(\frac{0.292}{0.208} \right)} = 1.345 \qquad \text{(B.7)}$$

This number is considerably smaller than the conductive heat-transfer coefficient as expected, because the tight spacing between tubing and casing walls precludes well-developed convection cells. Smaller than this though is the coefficient for radiative heat-transfer.

$$h_r = \frac{\sigma(T_{ci}^{*2} + T_{to}^{*2})(T_{ci}^{*} + T_{to}^{*})}{\frac{1}{\varepsilon_{ci}} + \frac{r_{ci}}{r_{to}}\left(\frac{1}{\varepsilon_{ci}} - 1 \right)} = \frac{1.713e-9 * (640^2 + 639^2)(640 + 639)}{\frac{1}{0.075} + \frac{3.5}{2.5}\left(\frac{1}{0.075} - 1 \right)} = 0.0586 \qquad \text{(B.8)}$$

The asterisks are reminders for using Rankine instead of Fahrenheit and ε is the emissivity (the ability to transmit energy in the form of radiation) of the bounding solid surface; it is specific to the material and measured relative to a black body's ability to emit radiation, therefore it is unitless (Massoud, 2005). The Stefan-Boltzmann constant has a value of 1.713×10^{-9} for units of

reciprocal ft^2-hr-°R (Hasan and Kabir, 2002). Combining these values allows for the overall heat-transfer coefficient to be computed.

$$\frac{1}{U_{to}} = \frac{0.208}{0.1875*1{,}495} + \frac{0.208*\ln(1.11)}{11.54} + \frac{0.208}{0.292*(1.345+0.0586)} + \frac{0.208*\ln(1.4)}{0.406}\cdots$$
$$+\frac{0.208*\ln(1.071)}{11.54} + \frac{0.208*\ln(1.13)}{4.021} = 0.6913\frac{hr\cdot ft^2\cdot °F}{Btu} \quad \text{(B.9)}$$

Therefore, the overall coefficient is 1.4465 Btu/hr-ft^2-°F at the bottom of the well; this is a reasonable number since there is little difference in temperature near the source of the fluid. The coefficient increases with elevation and is largest at the mud line.

Vita

James Thomas Stiernberg was born in Galveston, Texas, in 1986. Shortly thereafter, he moved to Bellaire, Texas for most of elementary school and graduated from Bellaire High School in 2004. He followed his two brothers, Charles and William, to the Cockrell School of Engineering at the University of Texas at Austin. He graduated with a Bachelor of Science in Geosystems Engineering and Hydrogeology in the spring of 2009. He promptly went to work for Halliburton as a surface data logging field engineer on deepwater drilling rigs in the Gulf of Mexico. In his final summer before graduating from Louisiana State University, he gained engineering experience during his internship with Chevron in Bakersfield, California; the company made a return offer, which he accepted. He enjoys rock climbing, running, swimming, electronics and art in his spare time.